



HAL
open science

A GIS-based Urban and Peri-urban Landscape Representation Toolbox for Hydrological Distributed Modeling

P. Sanzana, J. Gironas, Isabelle Braud, F. Branger, F. Rodriguez, X. Vargas, N. Hitschfeld, J.F. Munoz, S. Vicuna, A. Mejia, et al.

► **To cite this version:**

P. Sanzana, J. Gironas, Isabelle Braud, F. Branger, F. Rodriguez, et al.. A GIS-based Urban and Peri-urban Landscape Representation Toolbox for Hydrological Distributed Modeling. *Environmental Modelling and Software*, 2017, 91, pp.168-187. 10.1016/j.envsoft.2017.01.022 . hal-01826273

HAL Id: hal-01826273

<https://hal.science/hal-01826273>

Submitted on 29 Jun 2018

HAL is a multi-disciplinary open access archive for the deposit and dissemination of scientific research documents, whether they are published or not. The documents may come from teaching and research institutions in France or abroad, or from public or private research centers.

L'archive ouverte pluridisciplinaire **HAL**, est destinée au dépôt et à la diffusion de documents scientifiques de niveau recherche, publiés ou non, émanant des établissements d'enseignement et de recherche français ou étrangers, des laboratoires publics ou privés.

1 **A GIS-based Urban and Peri-urban Landscape Representation Toolbox for**
2 **Hydrological Distributed Modeling**

3 Sanzana, P.^{(1,2,5,*),} Gironás, J.^{(1,2,3,4),} Braud, I.^{(5),} Branger, F.^{(5),} Rodriguez, F.^{(6),} Vargas, X.^{(7),}
4 Hitschfeld, N.^{(8),} Muñoz J.F.^{(1),} Vicuña, S.^{(1,4),} Mejía, A.^{(9),} Jankowsky S.⁽¹⁰⁾

5

6 (1) Departamento de Ingeniería Hidráulica y Ambiental, Pontificia Universidad Católica de
7 Chile, Avenida Vicuña Mackenna 4860, Santiago, Chile.

8 (2) Centro de Desarrollo Urbano Sustentable CONICYT/FONDAP/15110020, Avenida
9 Vicuña Mackenna 4860, Santiago, Chile.

10 (3) Centro de Investigación para la Gestión Integrada de Desastres Naturales
11 CONICYT/FONDAP/15110017, Avenida Vicuña Mackenna 4860, Santiago, Chile.

12 (4) Centro Interdisciplinario de Cambio Global, Avenida Vicuña Mackenna 4860, Santiago,
13 Chile.

14 (5) IRSTEA, HHLY, Hydrology-Hydraulic Department, Centre de Lyon-Villeurbanne, 5 rue
15 de la Doua, BP32108, 69126 Villeurbanne, France.

16 (6) LUNAM Université, Institut Français des Sciences et Technologies des Transports de
17 l'Aménagement et des Réseaux (IFSTTAR), Département Géotechnique Eau et Risques et
18 Institut de Recherche en Sciences et Techniques de la Ville (IRSTV), F-44341 Bouguenais,
19 France.

20 (7) Departamento de Ingeniería Civil, Facultad de Ciencias Físicas y Matemáticas,
21 Universidad de Chile, Blanco Encalada 2002, Santiago, Chile.

22 (8) Computer Science Department, Facultad de Ciencias Físicas y Matemáticas,
23 Universidad de Chile. Av. Blanco Encalada 2120, Santiago, Chile.

24 (9) Department of Civil and Environmental Engineering, The Pennsylvania State
25 University, University Park, State College, PA 16802, USA

26 (10) Risk Management Solutions, Inc., Peninsular House, 30 Monument Street, London
27 EC3R 8NB UK

28

29 ***Corresponding author:** Av. Vicuña Mackenna 4860, Santiago, Chile; Voice: (56)
30 223545849; Fax: (56)-2- 23545876. Email: ppsanzana@uc.cl

31

32 **ABSTRACT**

33 Flowpaths are significantly affected by land use change and engineered elements across
34 urban catchments. Conventional GIS-based tools for extracting drainage networks were not
35 developed for urban terrains. This work presents Geo-PUMMA, a GIS toolbox to generate
36 vectorial meshes for terrain representation in distributed hydrological modeling, and to
37 extract drainage patterns in urban and peri-urban catchments. Geo-PUMMA generates well-
38 shaped Hydrological Response Units (HRUs) and Urban Hydrological Elements (UHEs).
39 The toolbox was used in peri-urban catchments of Chile and France to generate three model
40 meshes with different levels of treatment, and extract and compare their corresponding
41 drainage networks. A recommended mesh is identified, which replicates the main
42 morphological and hydrological features of the reference drainage network, and is able to
43 preserve features at small to medium spatial scales (~ 80 – 150 m). Overall Geo-PUMMA
44 can be used to represent the terrain in distributed hydrological modeling applied to urban
45 and peri-urban scales.

46 .
47

48 **Keywords:** Peri-urban catchments; Hydrological Response Units; Urban Hydrological
49 Elements; Drainage extraction; Computer-assisted mesh generation

50 SOFTWARE AVAILABILITY

51

52 Availability: <https://forge.irstea.fr/projects/geopumma>.

53 Additional technical documentation: A user manual with an example database available
54 from the same web address.

55 Year First Available: 2016

56 Hardware Required: Desktop/Laptop with 2 GHz CPU, 4 GB RAM or more

57 Operating System Required: Ubuntu 14 (64b) or newer

58 Software required: Geo-MHYDAS,-GRASS GIS 6.4, QGIS 2.12. These software and other
59 plugins and libraries are packaged in a Virtual Box Machine available from the same web
60 address

61 Cost: Free

62 Program Language: Python

63 License: GNU General Public License

64

65 Geo-PUMMA was developed in GRASS 6.4 in a virtual machine with Ubuntu 14 (64b).
66 Although programming skills are not needed, Geo-PUMMA requires some knowledge on
67 spatial analysis and hydrological modeling. It is necessary to be familiar with the use of
68 commands and to have basic knowledge of urban hydrology that allow making decisions
69 when representing urban features.

70 1. INTRODUCTION

71 Urban development significantly changes the hydro-geomorphology of natural river
72 catchments and their drainage networks (Booth and Henshaw, 2001; Booth and Fischenich,
73 2015; Vietz et al., 2015). Some of the most impacted areas are located in so-called peri-
74 urban catchments, where urban development is often ongoing, and natural, rural and urban
75 areas coexist (Santo Domingo et al., 2010). Peri-urban catchments are particularly
76 vulnerable to environmental change with urban development drastically modifying the
77 landscape (Lee and Heaney, 2003; Shuster et al, 2005) and changing the connectivity of
78 surface and sub-surface flowpaths (Braud et al., 2013). Thus, the accurate characterization
79 and representation for modelling purpose of these catchments becomes essential.

80 The representation of surface flowpaths at small scales is critical in hydrological
81 modeling of urban and peri-urban areas. Such representation must consider not only
82 channelized elements, but also the connectivity of impervious and pervious surfaces
83 (Sanzana et al., 2013; Rossel et al., 2014). In small catchments, surface routing is sensitive
84 to the presence of relatively small channels, which can be highly responsive to intense and
85 short rainfall events (Singh, 1995). Moreover, Rossel et al. (2014) showed that the
86 connectivity among pervious and impervious areas affects the magnitude and relative
87 contribution of the different mechanisms that ultimately influence the overall catchment
88 response. Finally, Jankowfsky (2011) showed how the use of inappropriate polygon meshes
89 to represent the terrain affects the correct connectivity of hydrological elements.

90 Several GIS tools have been developed to represent and visualize landscapes and
91 extract information for hydrological modeling. Classical methodologies of drainage
92 extraction and catchment delineation use Digital Elevation Models (DEM) and raster-based
93 flow direction algorithms, such as the D8 (O'Callaghan & Mark, 1984) or Multiple Flow
94 Directions (MFD) algorithm (Holmgren, 1994; Toma et al., 2001; Seibert and McGlynn,
95 2007). Furthermore, mathematical filters can be used with high-resolution DEM to detect
96 curvatures and slope directions, and define valleys and likely channelized locations in the
97 catchment (Lashermes et al., 2007; Passalacqua et al., 2010; Sangireddy et al., 2016). These
98 algorithms only extract well-defined streams and work fine in natural and non-flat areas at
99 regional or medium scales ($\sim 100\text{-}1000\text{ km}^2$), but tend to fail at smaller scales associated
100 with urban and peri-urban areas and catchments ($< 0.1\text{-}10\text{ km}^2$), where surface and

101 subsurface infrastructures can modify dramatically flow paths and catchments' boundaries
102 (Gironás et al., 2010; Jankowsky et al., 2013; Rodriguez et al., 2013). These tools
103 represent the terrain using cells of the same shape and size (e.g. square grid cells), but other
104 non-uniform meshes composed of triangles or polygons can also be used to avoid the
105 oversimplification of interfaces between hydrological elements, while reducing as much as
106 possible the number of elements in the final model mesh.

107 Good examples of GIS tools on raster-based are GRASS-HRU (Schwartz, 2008),
108 WINHRU (Viviroli et al., 2009) and GRIDMATH (Viviroli et al., 2009), and vector-based
109 are AVSWAT (Di Luzio et al., 2004), and PIHMgis (Bhatt et al., 2014). These tools use
110 Hydrological Response Units (HRUs) as elementary units, but they were developed to
111 represent medium and regional scale areas, so urban and peri-urban elements are normally
112 not well captured. Tanato2 (Bocher and Martin, 2012) is a GIS tool that uses Triangular
113 Irregular Networks (TINs) to represent complex urban and peri-urban terrains and their
114 special features and elements, as well as the interface between hydrological elements.
115 Nonetheless, the final mesh is composed only of triangles, and thus has notably more
116 elements than irregular meshes. Geo-MHYDAS (Lagacherie et al., 2010), a tool that uses
117 meshes conformed by irregular shape polygons developed for agricultural areas, is not
118 suitable for representing urban elements either, as it cannot deal with topological problems
119 typically found in urban terrain meshes (e.g., non-convex polygons, complex boundary
120 interfaces and large polygons).

121 Despite the afore mentioned advances in terrain representation for hydrological
122 modelling, the extraction of flow paths and the hydrological analysis of urban and peri-
123 urban environments handling man-made hydraulic features (e.g., ditches, channels and
124 pipes) is still an open scientific question. To the best of our knowledge, no specific tool is
125 available yet to generate good quality polygonal meshes for urban and peri-urban
126 catchment, i.e. a mesh composed of the least possible number of properly interconnected
127 well-shaped elements. A well-shaped element is a not-so-thin-and-slim pseudo-convex
128 polygon hydrologically homogenous, which allows the identification of the hydrologic
129 connectivity defined by the terrain, and ensure the efficient application of hydrological
130 models.

131 The objective of the paper is to present and illustrate the use of Geo-PUMMA, a
132 GIS tool to generate polygonal meshes for urban and peri-urban terrain representation, from
133 which a spatial characterization of the hydrological attributes, as well as an accurate
134 connectivity for distributed hydrological modeling, are obtained. After describing its
135 structure and main components, we illustrate an application of Geo-PUMMA for hydro-
136 geomorphological characterization of peri-urban catchments, with a particular focus on
137 their drainage network and its representation with different mesh alternatives whose quality
138 are assessed using geometrical and hydrological descriptors. Generally, the expression
139 “drainage network” refers to the network of pipes and streams conveying flow to the outlet.
140 In this paper, this concept refers to the whole connectivity structure among the hydrological
141 elements within the catchment contributing to the channelized system (streams, ditches and
142 sewer). Two catchments located in different landscapes and climatic conditions were
143 chosen: the Estero El Guindo catchment (Santiago, Chile), and the Mercier catchment
144 (Lyon, France).

145

146 2. Geo-PUMMA

147 2.1. General presentation of Geo-PUMMA

148 Geo-PUMMA is a semi-automatic toolbox to spatially represent urban and peri-
149 urban catchments and the explicit hydrological connectivity among their components, for
150 the subsequent implementation of semi-distributed and distributed hydrological modeling.
151 It uses a vectorial approach to produce irregular shape elements that are representative of
152 the principal physiographic units of small catchments (0.1-10 km²). Geo-PUMMA can
153 explicitly consider not only natural features, but also artificial infrastructures implemented
154 in urban and peri-urban environments (e.g., hydraulic infrastructure, detention and retention
155 devices, pipes and streets). Urban features are represented using Urban Hydrological
156 Elements (UHEs) (Rodríguez et al., 2008), while natural/rural areas are depicted using
157 Hydrological Response Units (HRUs) (Flügel, 1995). These units are represented using
158 varying-size, irregular shape polygons.

159 Geo-PUMMA builds upon the tools initially developed to process geospatial
160 information and represent peri-urban terrain in the hydrological model PUMMA
161 (Jankowfsky et al., 2014). This development is reported elsewhere in the literature (i.e.,

162 Paillé, 2010; Brossard, 2011; Jankowfsky, 2011; Sanzana et al., 2013). These tools were
163 developed using different computer languages and software (i.e. SQL, R scripts and
164 GRASS functions). Geo-PUMMA not only consolidates these tools in order to simplify
165 their use and the data processing, but also includes new functionalities. Geo-PUMMA is
166 implemented on the GRASS platform (GRASS Development Team, 2015) and QGIS
167 (Quantum GIS Development Team, 2015), and the corresponding codes are written in
168 Python programming language (python.org) due to the advantages of topological
169 management and available commands to process vector grids.

170 Geo-PUMMA considers four main steps covering the whole analysis process going
171 from data gathering and digitalization up to the derivation of the hydrological connectivity.
172 The first step (Step A) corresponds to data collection, digitalization and quality
173 improvement of all the geospatial maps relevant for the modeling of urban and peri-urban
174 hydrologic processes. The second step (Step B.1) corresponds to the description of the
175 urban area, in which all the UHEs are delineated and characterized using attributes such as
176 average height, area, percentage of imperviousness, green area, and distance from the
177 centroid to the closest sewer or street. In the third step (Step B.2) the initial HRUs
178 segmentation is improved using triangulation and dissolution processes based on the so-
179 called geometric indexes. In this step HRUs can also be segmented to lump the topographic
180 properties obtained from the DEM (Sanzana et al., 2013), including the slope, aspect, etc.
181 In the fourth step (Step B.3), the drainage network is extracted using a recursive algorithm
182 for identifying surface and sub-surface flow directions, and considering hydrological
183 connections among the different units. The obtained drainage network is composed of the
184 channelized infrastructure, natural streams and the entire connectivity among the HRUs and
185 UHEs draining to the channelized system (streams, ditches and pipes). A final step not
186 performed by Geo-PUMMA is needed to transform the geospatial features into database
187 tables to be processed by the hydrological model. For example, in the case of the PUMMA
188 model (Jankowfsky, 2011, Fuamba et al., 2015), this step uses SQL scripts developed by
189 Jankowfsky (2011). The resulting features can also be used in other models such as SWMM
190 (Gironás et al., 2010), SWAT (Neitsch et al., 2005), URBS (Rodriguez et al., 2008) or
191 MHYDAS (Moussa et al., 2002). Table 1 summarizes the different scripts implemented in
192 Geo-PUMMA, which can be of optional or compulsory use. The Geo-PUMMA Tutorial

193 (Geo-PUMMA Team, 2017) provides details and an example on how to use these scripts,
 194 that will give the user an idea of the computing times involved.

195 Although Geo-PUMMA is a self-contained tool including the scripts developed to
 196 implement this 4 step methodology, certain GRASS and Geo-MHYDAS scripts
 197 (Lagacherie et al., 2010) are needed for some specific steps, and should be installed
 198 together with Geo-PUMMA (Appendix 1 presents the main functions used in addition to
 199 Geo-PUMMA). From now on in the text, *m.script* and *v.function* correspond to external
 200 Geo-MHYDAS scripts and GRASS functions respectively. Readers are referred to the
 201 GRASS (GRASS Development Team, 2015) and Geo-MHYDAS (Lagacherie et al., 2010;
 202 Openfluid Project, 2016) documentation to learn about the use and implementation of these
 203 scripts. Nonetheless, a Virtual Box Machine with all the tools and external scripts is
 204 available from the Geo-PUMMA downloading site. More details and examples are
 205 available in the Geo-PUMMA Tutorial. What follows is a description of the four steps
 206 considered in Geo-PUMMA.

207

208 **Table 1. Tasks in each step of Geo-PUMMA and the corresponding scripts**

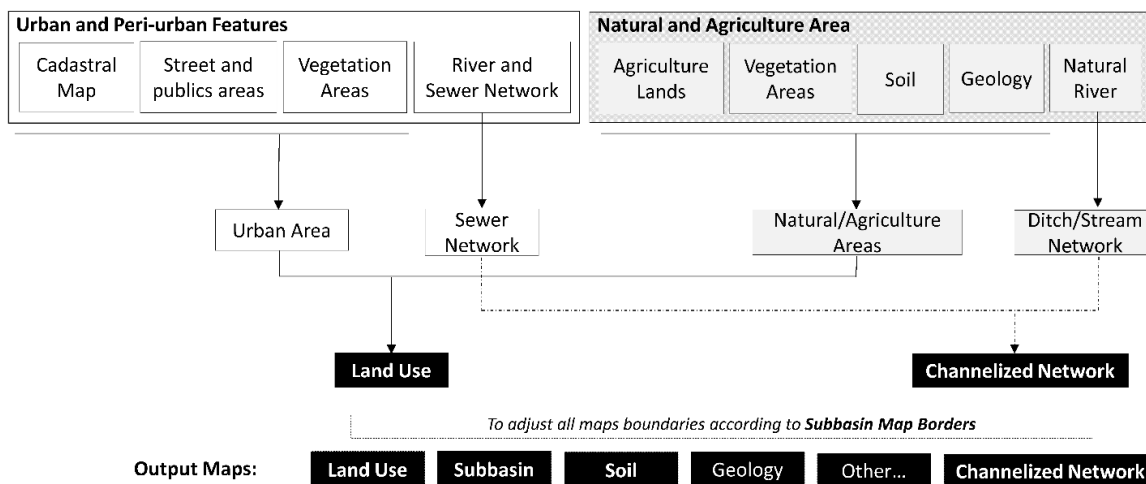
	Script/Plugin	Task (optional/compulsory)
Step A	<i>p.clean_topology.py</i>	Cleaning topological polygons (compulsory)
	<i>p.clean_polyline.py</i>	Snapping, breaking and joining polylines (optional)
Step B.1	<i>p.sidewalk_street.py</i>	Segmenting part of sidewalk and street in front of each urban lot (compulsory)
	<i>p.uhe.py</i>	Creating the UHE shapefile (compulsory)
	<i>p.a.average_altitude.py</i>	Getting the mean altitude and statistical parameters of each UHE (compulsory)
	<i>p.c.wood_surface.py</i>	Getting the green area percentage of each UHE (optional)
	<i>p.length.py</i>	Getting the distance from the centroid to the street centerline (compulsory)
	<i>p.built.py</i>	Getting the building percentage of each UHE (optional)
Step B.2	<i>p.polygons_holes.py</i>	Segmenting the HRU with island inside (optional)
	<i>p.shape_factors.py</i>	Calculating shape factors (convexity index, solidity index,

	Script/Plugin	Task (optional/compulsory)
		form factor and compactness) (compulsory)
	<i>Triangle Plugin</i>	Segmenting the bad-shaped HRU using library Meshpy and Software Triangle implemented in QGIS (compulsory)
	<i>p.convexity.py</i>	Dissolving using convexity and area criterion recommended for highly non-convex polygons (compulsory)
	<i>p.formfactor.py</i>	Dissolving using form factor and area criterion, recommended for thin and needle-shaped polygons such as streets (compulsory)
	<i>p.raster_segmentation.py</i>	Segmenting units with high variability of a given property from raster information (optional)
Step B.3	<i>p.all_interfaces.py</i>	Identifying all the interfaces between polygons and/or linear features (WTI and WTRI) (compulsory)
	<i>p.river_seg.m.py</i>	Segmenting the river considering the WTI and WTRI elements (compulsory)
	<i>p.wtri.py</i>	Identifying all interfaces between HRU/river and UHE/river (compulsory)
	<i>p.wti.py</i>	Identifying all interfaces between HRU/UHE (compulsory)
	<i>p.olaf.py</i>	Extracting the drainage network considering overland flow, natural streams and channelized infrastructures (compulsory)
	<i>p.geo_descriptors.py</i>	Updating the database from the model mesh, considering the update of distance and cumulative area as input for computing width and area functions (compulsory)
	<i>p.river_direction.py</i>	Changing all directions of the river's segments considering upstream (-1) or downstream (1) direction (optional)
	<i>p.rebuild_ditch_segments.py</i>	Dissolving all river segments, allows simplifying the number of final segments, keeping their properties uniform (optional)
	<i>p.river_h_s.py</i>	Getting the altitude and slope of each river segment (compulsory)

209

210 2.2. Step A: Data Collection and Maps Digitalization

211 The aim of Step A is to collect and pre-process all the relevant maps containing
 212 spatial information, including urban cadastral maps, land use maps, vegetation, soil type
 213 and geology layers, as well as natural and urban channelized networks (Fig.1). The pre-
 214 processing allows generating maps with clean topology to be used in the next steps. In
 215 addition to digitalized private and public lots, the cadastral maps should include public built
 216 areas (e.g., streets, squares and parks, sport and recreation areas, trails and bike paths).
 217 Certain infrastructures can be digitalized from high-resolution aerial photos, LiDAR (Light
 218 Detection and Ranging) images or similar, with resolutions finer than 0.5 m. Much of this
 219 information is available on-line, but some is found in urban data banks prepared and
 220 maintained by municipalities and public or private institutions. Green and natural areas as
 221 well as crops can be identified from satellite information and manually digitalized (Banzhaf
 222 et al., 2013; Jacqueminet et al., 2013). Finally, minor hydraulic infrastructure such as
 223 diversion elements, culverts and drains can be identified from field surveys.



224

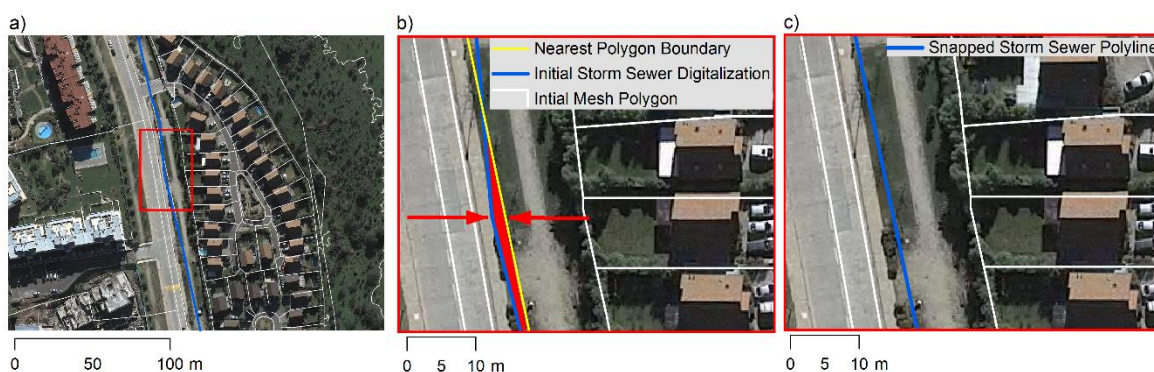
225 **Figure 1. Tasks and output maps associated with Step A, digitalization and pre-**
 226 **processing of input information**

227

228 Although most of the algorithms developed for remote sensing images consider a
 229 raster format, the resulting maps are vector layers (i.e., polygons, polylines). As expected,
 230 the quality of these maps and the subsequent computation of lumped properties such as
 231 height, slope and aspect, depend strongly on the resolution of the original DEM.

232 Once the basic polygonal layers have been collected, we recommend correcting
 233 linear elements such as rivers to avoid topological mistakes in the intersection step (Fig.2a),

234 in which all the polygon or polyline layers are overlapped. Thus, the channelized network
235 must be adjusted to one side of the street or to the closest edge elements to avoid the
236 creation of small irrelevant units for hydrological modeling (Fig.2b). Additionally, at this
237 step the edges of the lower resolution maps (e.g., soil type and geology) must be adjusted to
238 those with higher resolution (i.e., cadastral maps). Linear elements can only be adjusted
239 manually in a very time consuming manner given the length of channelized networks.
240 Nevertheless, as such correction is not included in Geo-PUMMA, we recommend using a
241 semi-automatic snapping tool such as the *m.snaplp* script, which allows snapping
242 automatically the vertex of the polyline to the nearest element (Fig.2c).



243
244 **Figure 2. Correction of linear elements to avoid topological mistakes when intersecting**
245 **different maps. (a) a particular urban location containing polygons from the initial**
246 **mesh (white polygons) and a digitalized storm sewer (blue polyline). (b) a sliver area**
247 **(red polygon) is created when intersecting the storm sewer and the initial mesh, which**
248 **can be removed by snapping the polyline to the nearest polygon boundary (yellow**
249 **line). (c) After the correction, the storm sewer overlaps the polygon boundary.**

250

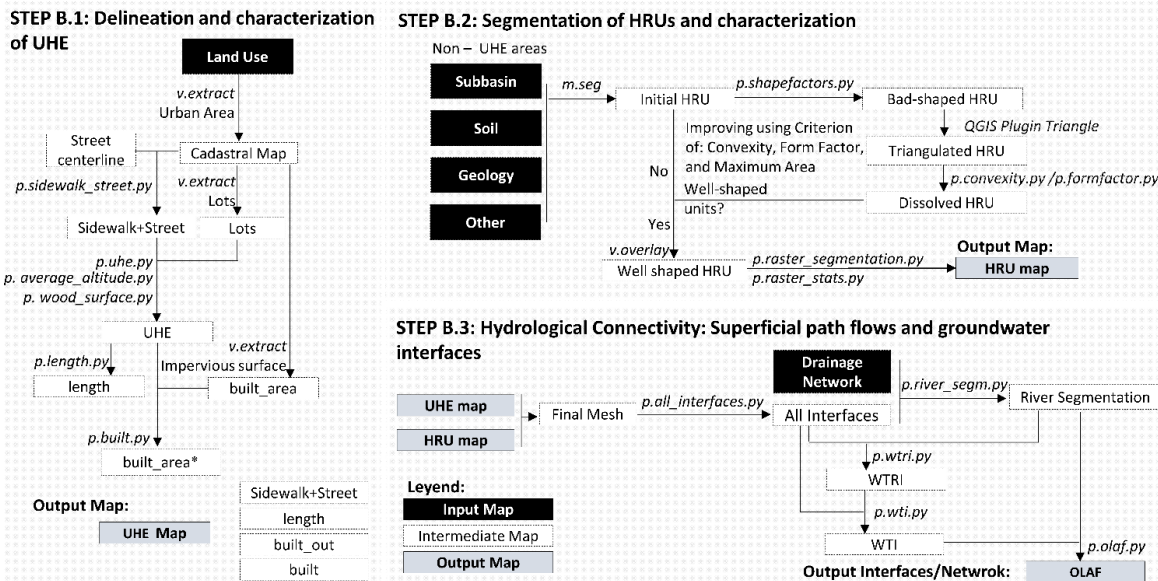
251 The next step is the delineation of the catchment and sub-catchment boundaries
252 using all the available related maps (e.g., land use, sub-catchments, soil and geology). If a
253 single stream network exists, the delineation based on the DEM can be a first
254 approximation, and drainage infrastructures (e.g., sewers and ditches) can be used later to
255 refine the boundaries. In fact, stormwater or combined sewer networks can hinder the
256 delineation and definition of urban sub-catchments, and field surveys become crucial to
257 achieve this task (Jankowsky et al. 2013). Finally, the limits of each of the input maps
258 must coincide exactly to generate the initial overlapped map. Each shapefile must be

259 imported into a GRASS database using *p.clean_topology.py* and *p.clean_polyline.py* to
260 avoid topological problems in polygonal and polylines features respectively.

261

262 2.3. Step B.1: Delineation and characterization of UHEs

263 To create the UHEs, urban lots, land plots and streets are first extracted from the
264 land-use layer (Fig. 3, step B.1) in which all the built elements are digitalized. A relevant
265 input for the definition of the UHEs is the polyline representing the axis of every street,
266 from which the distance to each UHE is computed. Because no specific script is available
267 in Geo-PUMMA, these street axes must be obtained from public or private database, or
268 digitalized from the urban street layer either manually or using computer-assisted tools
269 proposed elsewhere (Hu et al., 2004; Haunert and Sester, 2008; Leninisha and Vani, 2015).
270 Only scripts from Geo-PUMMA are needed to create the UHEs, and no extra tool is
271 required. The *p.sidewalk_street.py* script generates the sidewalk and street layer, and
272 identifies the sidewalk and half of the street in front of each lot. This layer and the cadastral
273 map are used by the *p.uhe.py* script to create the UHEs (see an example of final UHEs in
274 Fig. 4). Different scripts are then used to assign different attributes to each UHE, including:
275 average height (*p.average_altitude.py*), distance from the centroid to the center of the street
276 (*p.length.py*), built area in each lot (*p.built.py*), and the fraction of trees by lot
277 (*p.wood_surfaces.py*) in case a detailed digitalization of each lot is available. Alternatively,
278 Banzhaf et al. (2013) propose digitalizing the green areas of a random representative set of
279 lots to build a simple statistical relationship between the lot area and the percentage of
280 green area.



281

282 **Figure 3. Flowcharts showing Step B.1 (UHE characterization), Step B.2 (HRU**

283 **characterization) and Step B.3 (Hydrological connectivity description)**



284

285 **Figure 4. Example of UHEs generation in Geo-PUMMA. (a) Aerial Photography; (b)**

286 **Lot + Sidewalk + Middle of street in front of each lot, and (c) final UHEs map**

287

288 **2.4. Step B.2: Segmentation of HRUs**

289 **2.4.1. Initial HRUs**

290 The first step to obtain the initial HRUs is to intersect the main vector layers
 291 selected in Step A, excluding the UHEs. Usually, the tools to intersect layers in GIS
 292 platforms only operate with polygon layers (e.g. land use, sub-catchments, soil, and
 293 geology), but cannot intersect polygons with polylines (e.g. rivers and channels). Such
 294 capability is very relevant for peri-urban catchments. Thus, we propose using the script
 295 *m.seg*, although polygons features could also be intersected first, and subsequently the

296 polylines features could be manually used to cut the polygons they intersect. Subsequently,
297 the scripts *m.dispolygseg* and *m.sliverpolygseg* should be used to clean the resulting layers;
298 *m.dispolygseg* dissolves the smallest areas to a certain threshold value, whereas
299 *m.sliverpolygseg* dissolves areas with an elongated thin shape. One could also consider
300 using the GRASS function *v.clean*, although it dissolves all the longest boundaries of the
301 units below an area threshold.

302 The direct intersection of maps allows the identification of areas with homogeneous
303 properties, although the initial mesh is composed of elements of very irregular geometry.
304 As the distances between the centroid of the polygons are commonly used to represent the
305 mean flow distance among units, bad-shaped elements must be corrected to avoid affecting
306 hydrologic simulation. We define a good quality polygonal mesh for urban and peri-urban
307 catchments as a mesh composed of the least possible number of properly interconnected
308 well-shaped elements, with homogenous hydrological properties, that are representative of
309 the terrain and ensure the efficient application of hydrological models. Hence, the following
310 criteria must be satisfied (Sanzana et al. 2013): (1) the centroid must be inside each
311 element, (2) the boundaries must be smooth, (3) the area of each element must be in a
312 certain range, and (4) narrow and elongated elements must be avoided. In the following
313 subsections, we present the process to correct the bad-shaped elements.

314

315 2.4.2. Identification of bad-shaped HRUs

316 Bad-shaped elements can be identified after using the script *p.shapefactors.py*,
317 which computes for each HRU the geometric indexes Convexity Index ($CI = A_c/A$) and
318 Form Factor ($FF = 16A/P^2$), where A is the area of the polygon, A_c is the convex area and P
319 is the perimeter of the polygon. CI allows identifying HRUs with irregular shape in which
320 the centroid is generally outside, whereas FF allows identifying thin and long units. $CI = 1$
321 for regular shape polygons such as circles, squares and rectangles, whereas $CI < 1$ for any
322 non-convex units. On the other hand, $FF = 1$ for square polygons, and $FF < 1$ for thin and
323 long units. Finally, elements with a large area must be partitioned into new smaller areas.

324 A good quality mesh will be composed of well-shaped elements whose areas range
325 between a minimum and maximum value (A_{min} and A_{max} respectively), and for which CI
326 and FF are larger than certain threshold values CI_{min} and FF_{min} . First, the small elements

327 with no relevant physical significance must be dissolved by means of the *m.dispolygseg* or
328 *v.clean* scripts. A threshold area of $A_{min} = 10 \text{ m}^2$ is recommended for peri-urban landscapes.
329 Subsequently, elements with area larger than A_{max} must also be identified and segmented. A
330 value $A_{max} = 2 \text{ ha}$ is recommended for peri-urban areas. Second, elements with $FF < FF_{min}$
331 (i.e. narrow and thin units) and elements with $CI < CI_{min}$ are identified.

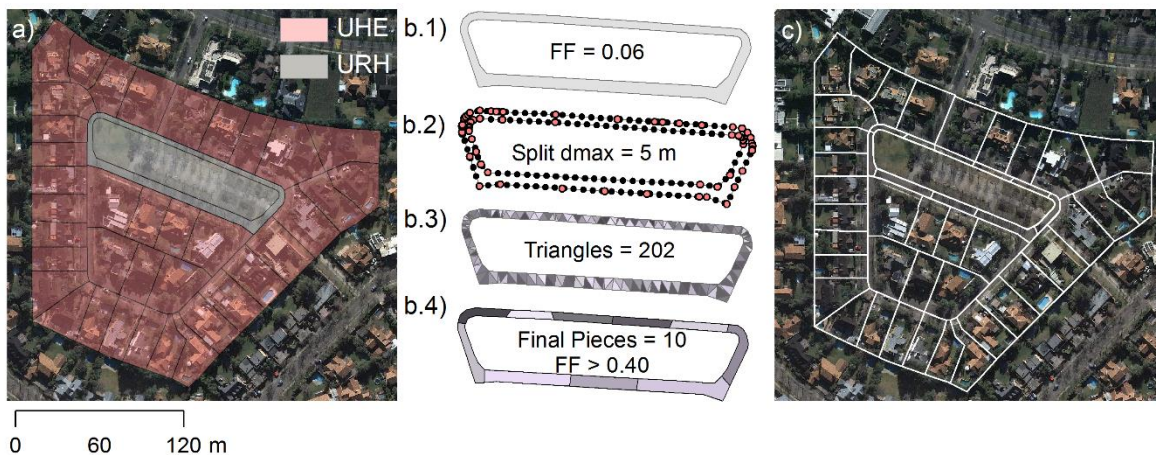
332 As a result, three independent bad-shaped subsets associated with the geometric or
333 area criteria are generated. The subset with small polygons ($A < A_{min}$) must be dissolved and
334 is not considered in the segmentation procedure. Because the bad-shaped units will be
335 triangulated to avoid increasing the processing times, the user must verify that the number
336 of vertexes of each subset does not exceed a certain value using the *v.info* script. We
337 suggest a maximum of 500 vertexes/ha to represent spatial features such as green areas.
338 Nevertheless, the function *v.generalize* can be used to simplify those elements in GRASS,
339 with its option for reducing the number of vertexes in a boundary using either the Douglas-
340 Peucker (Douglas and Peucker, 1973) or Snakes (Kass et al., 1988) algorithm.

341

342 2.4.3. Improvement of bad-shaped HRUs

343 To improve bad-shaped units Geo-PUMMA uses a divide and conquer approach, in
344 which the bad-shaped HRUs are segmented into a subset of triangles using the software
345 *Triangle* (Shewchuck, 1996) prior to grouping new well-shaped units. Two options are
346 considered for triangulation: (1) *R* scripts developed by Sanzana et al. (2013) to compile
347 *Triangle*, or (2) the *Triangle Plugin* available in QGIS, which uses the *Meshpy* library to
348 perform a triangulation over the shapefiles. Finally, the triangulated subset obtained using
349 the convexity criteria ($CI > CI_{min}$) is dissolved utilizing the *p.convexity.py* script, whereas
350 the *p.formfactor.py* script is used for the subset obtained using the form factor criteria ($FF >$
351 FF_{min}). The divide and conquer algorithm allows the segmentation using not only a
352 convexity criterion already presented in Sanzana et al. (2013), but alternatively a form
353 factor criterion developed especially for Geo-PUMMA, whose pseudo-code is presented in
354 the Appendix 2 and illustrated in Fig. 5. The urban area in Fig.5a includes a street
355 surrounding a square, which corresponds to a bad-shaped element with $FF = 0.06$
356 (Fig.5b.1). The segmentation of this polygon considers adding vertexes every 5 m or less
357 (Fig.5b.2), the subsequent triangulation (Fig.5b.3) and dissolving to generated 10 pieces

358 with $FF > FF_{min} = 0.4$ (Fig.5b.4). Finally the new mesh is composed of well-shaped and
359 small elements (Fig 5c).



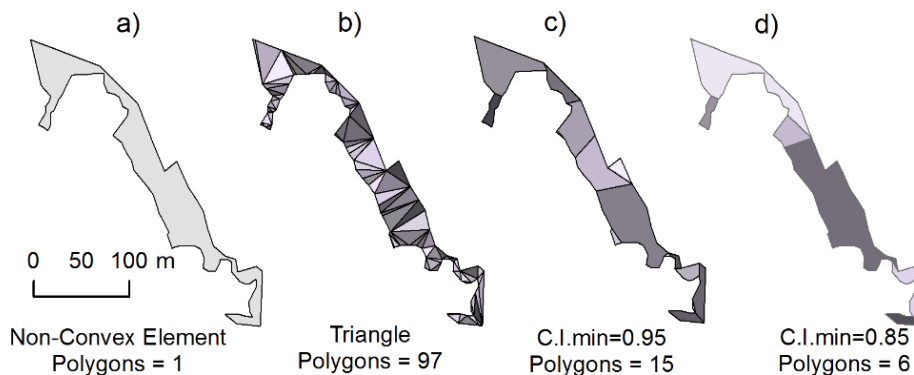
360

361 **Figure 5. An example of a bad-shaped polygon improvement. (a) a long and**
362 **thin street surrounding a square is generated. (b) The street corresponds to a bad-**
363 **shaped polygon with $FF = 0.06$, which is treated to generated 10 elements with $FF >$**
364 **$FF_{min}=0.4$. (c) final improved mesh.**

365

366 This process produces a good quality mesh made up of well-shaped elements that
367 still may have small area units and/or elongated triangles. A new application of the
368 *p.shapefactors.py* routine allows identifying units with $A < A_{max}$, $CI < CI_{min}$ and $FF < FF_{min}$
369 values. The iterative application of the divide and conquer approach using *CI* or *FF* criteria
370 can produce new small bad-shape elements, as these criteria may sometimes not be
371 compatible. Small elements without hydrological meaning are finally dissolved, whereas
372 the others are kept in the final mesh despite not fulfilling the geometric criteria.

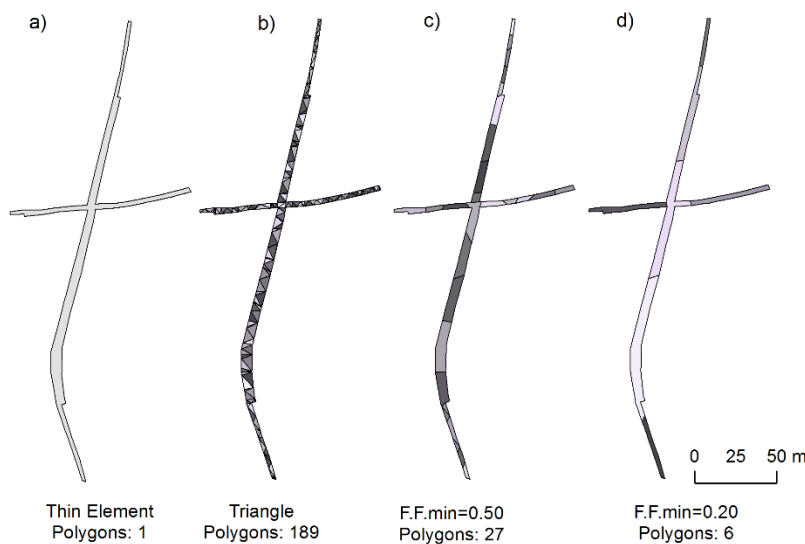
373 Fig. 6 illustrates the use of the script *p.convexity.py* in the segmentation of a bad-
374 shaped unit. The unit (Fig. 6a) is divided in triangulated units (Fig. 6b), which are dissolved
375 into polygons using threshold values of $CI_{min} = 0.95$ (Fig. 6c) and $CI_{min} = 0.85$ (Fig. 6d). Fig.
376 7 illustrates the use of the script *p.formfactor.py* in the segmentation of a bad-shaped unit
377 with a thin and long shape. The thin element (Fig. 7a) is divided in triangulated units (Fig.
378 7b) that are dissolved into polygons using threshold values of $FF_{min} = 0.50$ (Fig. 7c) and
379 $FF_{min} = 0.20$ (Fig. 7d).



380

381 **Figure 6. HRU segmentation according to Convexity Criterion. Initial Polygon (a),**

382 **Triangulated Polygon (b), Dissolved with $CI_{min} = 0.95$ (c) and $CI_{min} = 0.85$ (d)**



383

384 **Figure 7. HRU segmentation according to Form Factor Criterion. Initial Polygon (a),**

385 **Triangulated Polygon (b), Dissolved with $FF_{min} = 0.50$ (c) and $FF_{min} = 0.20$ (d)**

386

387 2.4.4. Segmentation by raster criterion

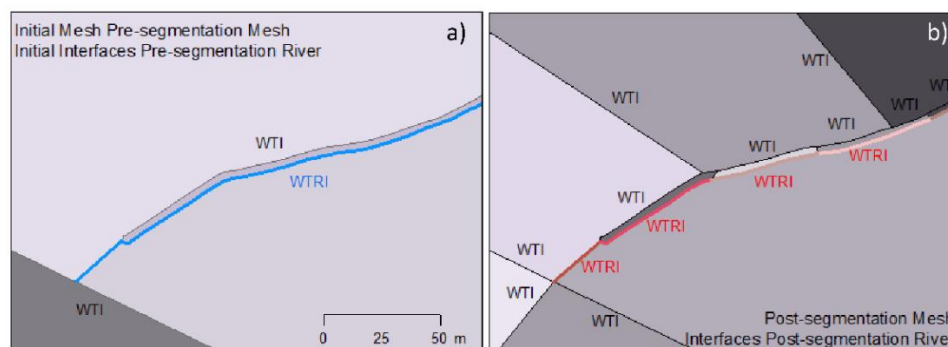
388 The final segmentation step using the *p.raster_segmentation.py* routine (Sanzana et
389 al., 2013) is applied to the HRUs with high internal variability of topographic attributes,
390 such as slope or aspect. This script creates new more homogeneous units and facilitates the
391 extraction of a more realistic hydrological connectivity.

392

393 2.5. Step B.3: Hydrological connectivity

394 The hydrological connectivity of surface flow paths and subsurface interfaces is
395 extracted from the improved mesh (Fig. 3, Step B.3). Routing algorithms are applied
396 considering the centroid of the units directly connected to the drainage system. The length
397 of the interface between adjacent units is used to estimate the lateral subsurface flow
398 between two units (HRU or UHE) or between one unit and the river. The hydrological
399 interfaces are identified using the *p.all_interfaces.py* routine. Then, the initial river (Fig. 8a)
400 is segmented based on the boundary of the adjacent units using the *p.river_segm.py* routine
401 (Fig. 8b). In addition, the *p.wti.py* and *p.wtri.py* scripts are used to identify all the interfaces
402 through which flow exchange between the river and neighboring units occurs. These
403 interfaces are defined as WTRI (Water Table River Interfaces) and WTI (Water Table
404 Interfaces) (Fig. 8b).

405



406

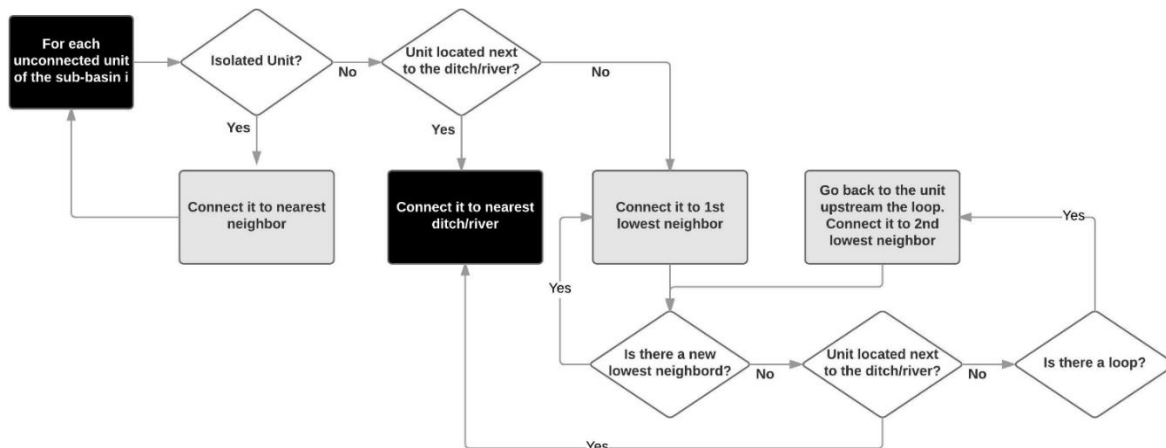
407 **Figure 8. Initial River (a) and Segmented River (b) based on HRU neighbors**

408

409 The *p.olaf.py* routing algorithm (Brossard, 2011) connects first all river segments
410 bordering HRUs and all the isolated HRUs with only one neighbor. Then, for the remaining
411 HRUs, it looks for the minimal height until reaching the river or channel section. As a
412 result, a vector layer with the hydrological connectivity of the HRUs and UHEs is obtained.
413 If a loop is generated within the process, the algorithm recursively looks for an alternative
414 route from the unit starting the loop until reaching the drainage system (the pseudo-code of
415 the OLAF algorithm is presented in Appendix 3, its flowchart in Fig. 9 and an example of
416 application in Fig. 10). Because the sub-catchments are delineated as an intermediate step,
417 the search is only carried out inside each sub-catchment, and avoids leaps to neighboring
418 catchments as the topographic boundaries previously imposed are respected. The *p.olaf.py*

419 algorithm also delivers the HRUs subset that could not be connected to the general system.
420 In this case, the heights must be verified and the routine run again. A manual checking and
421 connection is eventually needed only when bad-shaped elements or big flat units produced
422 by the previous segmentation still remain.

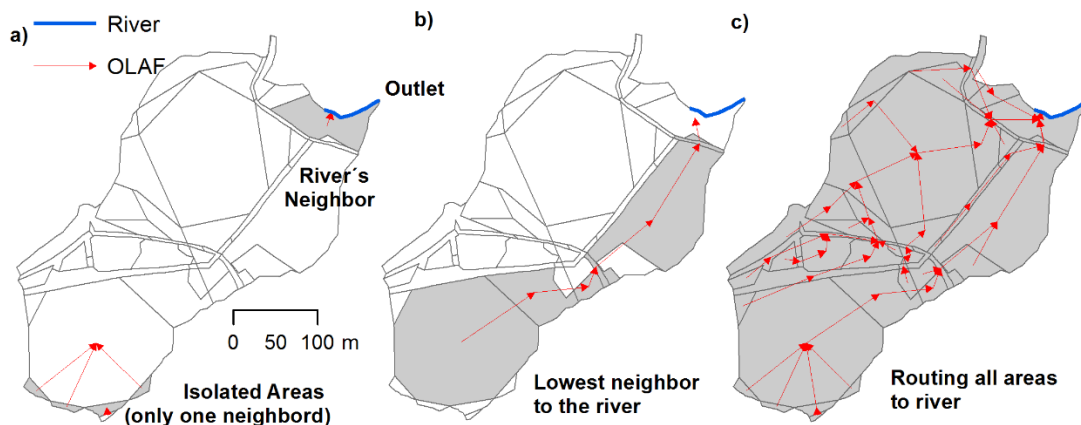
423 The *p.geo_descriptors.py* routine can be used to perform a detailed analysis of the
424 spatial distribution of the connected area. This routine stores the area -or any other property
425 whose value is spatially distributed- and distance to the outlet point. This information can
426 then be used to compute the width and area function, two geomorphological functions
427 utilized later to characterize the drainage networks generated by Geo-PUMMA. In a final
428 step, the direction of the drainage system can be defined from downstream or upstream
429 with the *p.river_direction.py* script. Furthermore, in order to minimize the number of
430 stream reaches and reduce computation time, portions of them with similar characteristics
431 (particularly height) can be dissolved with *p.rebuild_ditch_segments.py*, while the height
432 and slope are reassigned with the *p.river_h_py* script.



433

434 **Figure 9. OLAF algorithm flowchart.**

435



436

437 **Figure 10. An example of the OLAF algorithm. a) Connection of neighboring river**
438 **units to the river and isolated polygons with neighbor polygon, b) routing upper units**
439 **into downstream unit and c) routing until connecting all units**

440

441 3. APPLICATION OF Geo-PUMMA TO TWO CASE STUDIES

442 As an application example, Geo-PUMMA was implemented in two peri-urban
443 catchments located in different geographical regions, to create and geomorphologically and
444 hydrologically compare 3 particular meshes generated by the model and the corresponding
445 drainage networks. This application illustrates the performance and flexibility of Geo-
446 PUMMA when used in diverse landscapes with different data availability and format, and
447 allows recommending strategies and parameter values to obtain good-quality meshes. In
448 addition, the final segmentation obtained with Geo-PUMMA is qualitatively compared
449 against the application of a traditional raster-based approach, in order to show the
450 advantage of the Geo-PUMMA vectorial approach. As a reference, the application of Geo-
451 PUMMA to the study catchments here described implied computing times of ~60 h.

452

453 3.1. Study areas and available information

454 3.1.1. Estero el Guindo catchment, Santiago (Chile)

455 The Estero El Guindo catchment (Fig. 11a) is located in the Andean foothill, in a
456 rapidly expanding peri-urban area in the piedmont of Santiago, Chile (Romero et al., 1999;
457 Romero and Vasquez 2005; Romero et al., 2010; Pavez et al., 2010; Banzhaf et al., 2013).
458 The catchment has an area of 6.5 km² and elevations range between 788 and 1310 m. The
459 geology is composed of permeable layer of fluvial deposits with andesitic rocks in the

460 impermeable bottom. There is an unconfined aquifer with shallow depths in the upper
461 portion of the catchment and larger depths in the lowest part. The natural area is covered by
462 native vegetation (51%) and the urban area covers the remaining 49%.

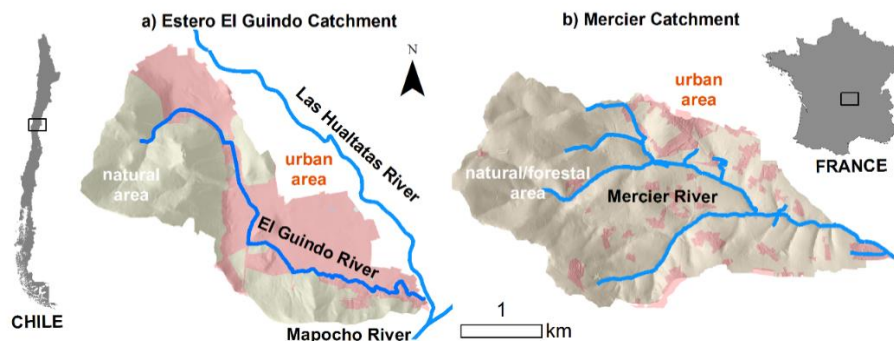
463 The land use map was generated using information provided by the Chilean Areal
464 Photographical Service and the Municipal Master Plan (Municipalidad de Lo Barnechea,
465 2012) whereas soil types and geology information were obtained from technical studies
466 (DGA-AC, 2000; DGA-Arrau, 2008). Contours every 1 and 2.5 m and 1:2,500 and 1: 5,000
467 maps were available from DOH-EIC (2004) for the urban and natural portions of the
468 catchment, respectively. Finally, the channelized network was identified from field surveys,
469 and information provided by DOH-CADE (2001) and DOH-EIC (2004).

470

471 3.1.2. Mercier catchment, Lyon (France)

472 The Mercier catchment (Fig. 11b) is part of the Yzeron peri-urban watershed (150
473 km²) located southwest of Lyon, France. It has an area of 6.8 km² and elevations range
474 between 300 and 785 m. The geology consists mainly of gneiss and granite, and soils are
475 quite shallow, especially in upslope areas, leading to an overall low water storage capacity.
476 Fifty percent of its area is for agriculture, 40% is covered by forests, and 10% is either
477 urban or impervious (Braud et al., 2013).

478 The available information includes a detailed land use map obtained by manual
479 digitalization (Jacquemet et al., 2013), a pedology map (SIRA, 2011), a geology map
480 (BRGM, 2011), a 2 m DEM (Sarrazin, 2012), a sub-catchment map generated using the
481 method proposed by Jankowsky et al. (2013), maps with ditches (Jankowsky, 2011), and
482 the sewer network provided by the Syndicat Intercommunal pour l'Aménagement de la
483 Vallée de l'Yzeron.



484

485 **Figure 11. Study areas. a) Estero el Guindo Catchment, Chile, and b) Mercier**
486 **Catchment, France.**

487

488 3.2. Modeling meshes and associated drainage networks

489 In this application, three meshes are defined:

- 490 • Initial Mesh (IniM): this mesh is obtained from intersecting the land use, soil type,
491 sub-catchments and geology layers, but without applying step B2 on HRUs. CI and
492 FF values for this mesh are not restricted, and thus no correction to the mesh
493 elements is implemented.
- 494 • Reference Mesh (RefM): this mesh was created using high values of the geometric
495 indexes, i.e. $CI_{min} = 0.975$, $FF_{min} = 0.5$, and $A_{max} = 2$ ha. This is the best model mesh
496 to be obtained from the available information, which allows the best topographic
497 fidelity while avoiding topological problems. This mesh ensures a high degree of
498 segmentation and significantly increases the number of final elements.
- 499 • Recommended Mesh (RecM): This mesh is obtained when using the default values
500 of $CI_{min} = 0.75$, $FF_{min} = 0.20$ and $A_{max} = 2$ ha. This mesh is a compromise between
501 the initial and reference meshes. It relies on CI and FF values that allow getting
502 well-shaped elements, without significantly increasing their number.

503

504 3.3. Characterization and assessment of the meshes and drainage networks

505 3.3.1. Width and area functions

506 To characterize the drainage network extracted from each mesh, we use the width
507 function $W(x)$ and area function $A(x)$. $W(x)$ corresponds to the number of drainage segments
508 located at a given distance x from the catchment outlet along the drainage network, whereas
509 $A(x)$ is the portion of contributing area associated to this flow distance x (Rodríguez-Iturbe
510 and Rinaldo, 1997). Both $W(x)$ and $A(x)$ allow the characterization of the arrangement of
511 flow paths and contributing areas in the catchment, which have strong implications on its
512 hydrologic response (Rodríguez-Iturbe and Rinaldo, 1997). Indeed, $W(x)$ has previously
513 been used to compare drainage network representations (Richards-Pecou, 2002; Moussa,
514 2008; Rodríguez et al., 2013; Sanzana et al., 2013), and to assess the effect of urbanization

515 on the drainage network structure and potential impacts in the resulting hydrograph
516 response (e.g., Smith et al., 2002; Gironás et al., 2009; Ogden et al., 2011).

517 In particular, we compare $W(x)$ and $A(x)$ of the IniM and RecM against the RefM to
518 identify the locations and spatial scales at which the drainage networks associated with the
519 different meshes differ. To assess the goodness-of-fit against the RefM, we use the Mean
520 Absolute Error (MAE) and the Nash-Sutcliffe efficiency coefficient (C_{NS} , Nash and
521 Sutcliffe, 1970). The MAE is a residual measure to evaluate the goodness-of-fit in the units
522 of the variable (Bennet et al., 2013), whereas the C_{NS} is a relative error measure, which
523 combines the correlation coefficient and observed and simulated means and standard
524 deviations, to assess similarities in the overall function patterns (Legates and McCabe,
525 1999; Bennet et al., 2013). Values of $C_{NS} < 1$ are associated with differences in the
526 connectivity of the modeling meshes.

527 Because both $W(x)$ and $A(x)$ allow reducing the 2D drainage structure to a 1D
528 mathematical function, they can be analyzed and compared using power spectral analysis.
529 This analysis quantifies the distribution of power per unit frequency of discrete series, and
530 is a useful tool to get information about their structure in the frequency domain. Such
531 analysis has been previously applied to $W(x)$ and/or $A(x)$ (Rodríguez-Iturbe and Rinaldo,
532 1997; Veneziano et al., 2000; Richards-Pecou, 2002; Puente and Sivakumar, 2003; Moussa,
533 2008; Sanzana et al., 2013). For each of the three meshes, we compare the cross power
534 spectral density (CPSD) of $W(x)$ (and $A(x)$) against that of $W(x)$ (and $A(x)$) of the RefM.
535 The CPSD is the power spectral of the cross-covariance between two series (Shynk, 2012),
536 which allows quantifying the power shared by a given frequency for the two series. Hence,
537 it can be used to identify at which spatial scales $W(x)$ (and $A(x)$) of the IniM and RecM
538 differ from $W(x)$ (and $A(x)$) of the RefM. Note that the CPSD of the same series is simply
539 the power spectral density of the series. All the CPSD were computed using Matlab®.

540

541 3.3.2. Instantaneous Unit Hydrograph (IUH)

542 The basin geomorphology has been proven to be closely linked to its hydrologic re-
543 sponse (Rodríguez-Iturbe and Rinaldo, 1997). In particular, $A(x)$ incorporates some essen-
544 tial characters of the hydrologic response because the travel time from the subareas in the
545 catchments is related to the flow distance to be traversed. Thus, by normalizing $A(x)$ to ob-

546 tain a unit area under the curve, and defining constant overland and channelized flow veloc-
 547 ities, the spatial scale of $A(x)$ can be transformed into a temporal scale to generate an in-
 548 stantaneous unit hydrograph (IUH), i.e. the hydrologic response of the basin when repre-
 549 sented as a linear system. This transformation has been implemented elsewhere in the liter-
 550 ature (e.g. Rinaldo et al. 1995, Morrison and Smith, 2001, Smith et al., 2005; Gironás et al.
 551 2009) and is proposed here to better understand the hydrologic impacts of the catchment
 552 representation using different modeling meshes computed by Geo-PUMMA. Following
 553 what is proposed by the UDFCD (2006), for Estero El Guindo we adopted a velocity $V_H =$
 554 0.75 m/s for natural hillslopes or HRU (mean slope 34%), a velocity $V_U = 0.27$ m/s for ur-
 555 ban areas or UHE (mean slope 7%) and a velocity $V_{Ch} = 2.2$ m/s for the channelized net-
 556 work (mean slope 3%, mixed natural/concreted channel). For the Mercier we adopted val-
 557 ues of $V_H = 0.27$ m/s (mean slope 13%), $V_U = 0.60$ m/s (mean slope 8%) and $V_{Ch} = 1.85$ m/s
 558 (mean slope 9%, mostly natural channel).

559

560 3.3.3. Discretization error metric

561 Finally, we also use the sub-basin discretization error metric ΔL_s associated with a
 562 certain schematic representation s (Liu et al., 2016) to compare IniM and RecM against
 563 RefM. ΔL_s is given by:

$$564 \quad \Delta L_s = L_o - L_s = \frac{\sum_{i=1}^n A_{io} L_{io}}{\sum_{i=1}^n A_{io}} - \frac{\sum_{j=1}^m A_{js} L_{js}}{\sum_{j=1}^m A_{js}} \quad (1)$$

565 where L_o and L_s are the area-weighted in-channel routing lengths of the reference schematic
 566 representations o and the representation s , and A_{io} (A_{js}) is the areas contributing to the
 567 routing channel i (j) of representation o (s), whose length is L_{io} (L_{js}). Although originally
 568 proposed for channelized network, this error metric can be used with meshes in which the
 569 different subareas have their corresponding drainage segment. Note that ΔL_s is a priori
 570 discretization error metric to estimate the hydrologic information loss by any discretization
 571 scheme as compared to a reference discretization (Liu et al., 2016). Hence, this metric
 572 complements the computation and analysis of the IUH in quantifying the hydrologic impact
 573 of different terrain representations without running a comprehensive hydrologic model.

574

575 4. RESULTS AND DISCUSSION

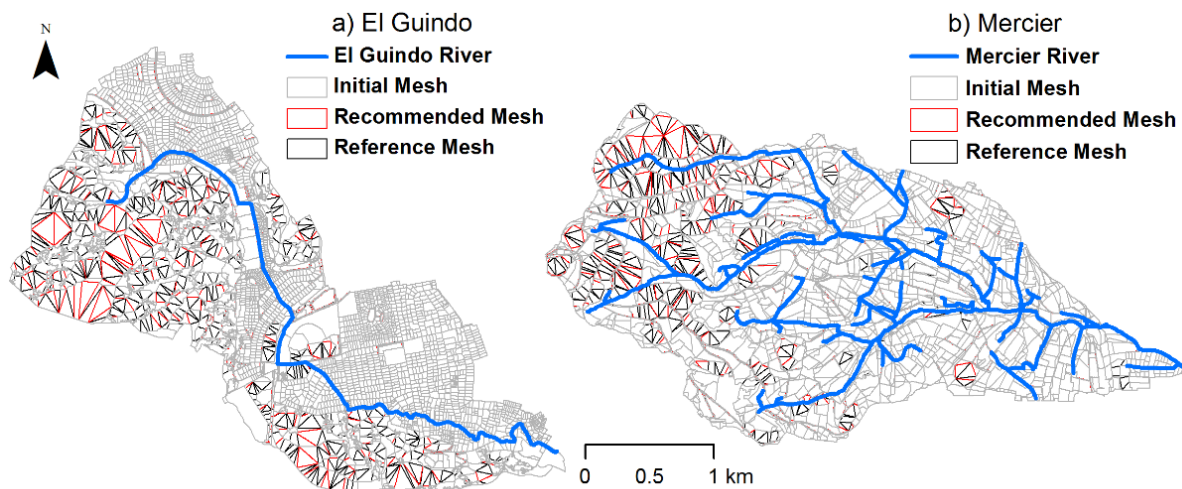
576 4.1. Main characteristics of the various modeling meshes

577 Fig. 12 shows the three meshes generated for the Estero El Guindo catchment (Fig.
578 12a) and Mercier catchment (Fig. 12b). Grey lines represent the initial polygon
579 segmentation (IniM), red lines the recommended mesh (RecM), and black lines the
580 reference mesh (RefM). The corresponding drainage networks of El Guindo and Mercier
581 are presented in Fig. 13. For each mesh, the drainage density (D_d), defined as the ratio
582 between the total length of the drainage network and the total area of the catchment, was
583 computed (Table 2). For the Estero El Guindo, the segmentation procedure increases D_d
584 from 24.2 km/km² (IniM) to 32.9 km/km² (RefM), while for RecM, $D_d = 26.2$ km/km². For
585 the Mercier catchment, the segmentation procedure increases the drainage density from
586 23.6 km/km² (IniM) to 31.6 km/km² (RefM), while for RecM, $D_d = 26.4$ km/km². In both
587 cases, D_d of the RecM increases by ~10% as compared to the IniM. This increase is ~30%
588 for the highly detailed segmentation of the referenced mesh. Thus, RefM improves the
589 representation of flow paths without increasing significantly the drainage density of the
590 initial mesh. The segmentation procedure increases the drainage density of both catchments
591 as the final number of hydrological response units also grows up. In addition, the increase
592 of hydrological connectivity allows avoiding topological problems in the drainage network,
593 due to the improvement of the flow paths representation.

594 Table 2 summarizes the main characteristics of the HRUs for each mesh, including
595 their number, minimum, maximum and average areas (A_{min} , A_{max} , A_{ave}), and the number of
596 well-shaped HRUs for which $CI_{min} > 0.75$ and $FF_{min} > 0.20$ (i.e. $HRU_{FF>0.2}$ and $HRU_{CI>0.75}$).
597 Furthermore, regardless of the mesh, there are 2169 UHEs for El Guindo catchment and
598 290 for the Mercier catchment. The UHEs are considered as well-shaped elements, so they
599 are preserved in all meshes. The segmentation of non-convex, thin and very large HRUs
600 produces meshes RecM and RefM that are more homogeneous than IniM, as reflected by
601 the increase in $HRU_{FF>0.2}$ and $HRU_{CI>0.75}$. Although in some cases the initial percentage of
602 well-shaped elements is high (e.g., IniM Mercier $HRU_{CI>0.75} = 99\%$), they can be relevant
603 in terms of area, so they must be included and improved to avoid connectivity distortions in
604 the drainage networks. Such improvement ensures a more representative overland flow

605 connectivity. For example, the segmentation removes long streets acting like walls that
606 artificially interfere the flow routing (Jankowfsky, 2011). Overall, Geo-PUMMA creates a
607 good quality mesh and a representative drainage network that can be useful for any
608 hydrological model applied to urban and peri-urban landscapes.

609



610

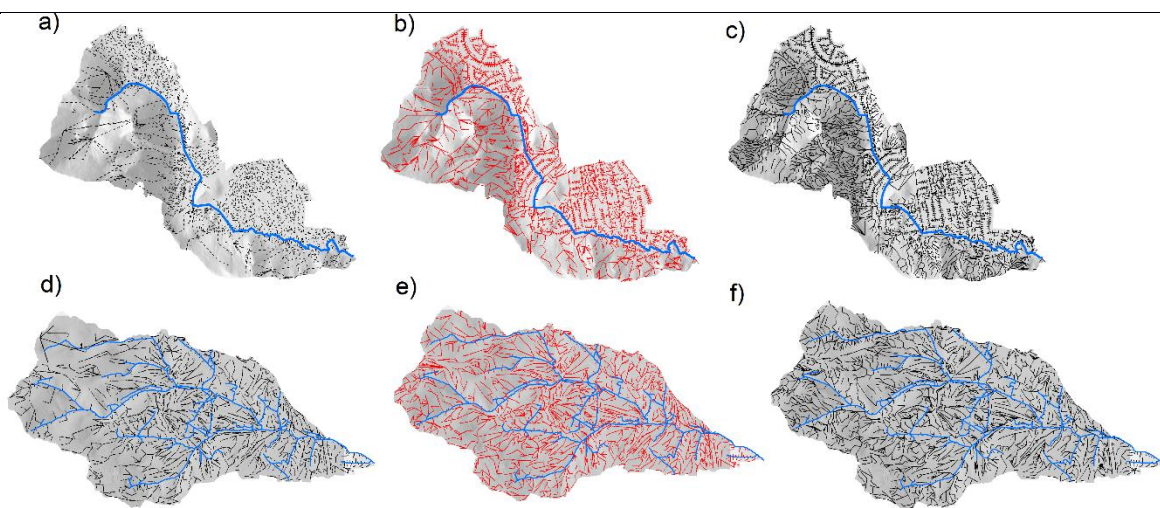
611 **Figure 12. Modeling meshes for El Guindo (a) and Mercier (b) catchments: Initial**
612 **(grey), Recommended (red), and Reference (black) segmentation units are identified**

613

614

615 **Table 2. Main characteristics of the Initial Mesh (IniM), Recommended Mesh (RecM)**
 616 **and Reference Meshe (RefM) obtained for the Mercier and El Guindo Catchments**

Mesh	$D_d(\text{km}/\text{km}^2)$	HRU	$A_{\min} (\text{m}^2)$	$A_{\max} (\text{m}^2)$	$A_{\text{ave}} (\text{m}^2)$	$\text{HRU}_{\text{FF}>0.2}$	$\text{HRU}_{\text{CD}>0.75}$
IniM El Guindo	24.2	2,057	0.1	243,133	2,119	767 (83.8 %)	737 (80.5 %)
RecM El Guindo	26.2	2,016	10	38,663	1,862	1,270 (94.9 %)	1,145 (85.5 %)
RefM El Guindo	32.9	3,749	10	29,466	1,427	2,370 (98.4 %)	2,229 (92.6 %)
IniM Mercier	23.6	915	2.0	192,144	3,118	1,644 (79.9%)	2,037 (99.0 %)
RecM Mercier	26.4	1338	10	20,275	2,354	1,849 (91.7 %)	1,998 (99.1%)
RefM Mercier	31.6	2408	10	19,337	1,811	3,480 (92.8%)	3,745 (99.8 %)



617 **Figure 13. Initial (a), Recommended (b), and Reference (c) Drainage Networks of El**
 618 **Guindo. Initial (d), Recommended (e), and Reference (f) Drainage Networks of**
 619 **Mercier**
 620 **Mercier**

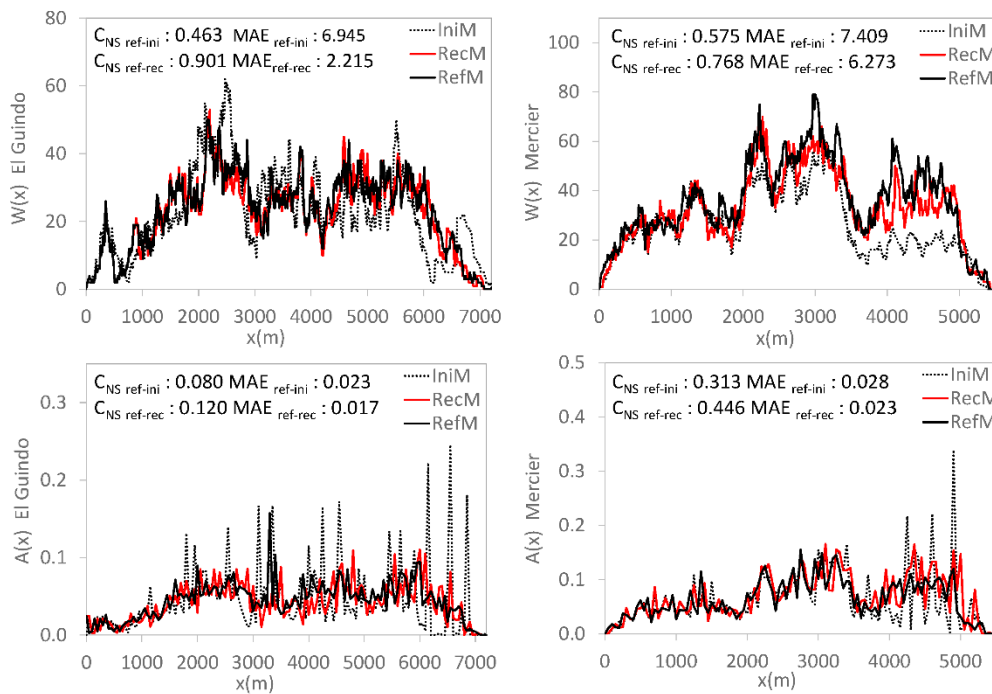
621
 622 4.2. Assessment and comparison of drainage networks

623 4.2.1. Width and area functions

624 Fig. 14 compares $W(x)$ and $A(x)$ of each mesh and catchment. $W(x)$ of IniM
 625 significantly differs from that of the RefM for Estero El Guindo ($C_{NS \text{ ref-ini}} = 0.463$ and $\text{MAE}_{\text{ref-ini}} = 6.95$, Fig.14a) and Mercier ($C_{NS \text{ ref-ini}} = 0.575$ and $\text{MAE}_{\text{ref-ini}} = 7.41$, Fig.14b), whereas
 626 such difference is much less substantial when comparing RecM and RefM, both in Estero
 627 El Guindo ($C_{NS \text{ ref-rec}} = 0.901$ and $\text{MAE}_{\text{ref-rec}} = 2.22$, Fig.14a) and Mercier ($C_{NS \text{ ref-rec}} = 0.768$
 628 and $\text{MAE}_{\text{ref-rec}} = 6.27$, Fig.14b). In the case of the Mercier catchment, $W(x)$ of IniM and
 629 RecM considerably differ in the upper part (from $x = 3500$ to 5200 m, Fig. 14b), as the
 630

631 segmented HRUs are mainly located in natural sections at the foothill area of the catchment
 632 (Fig.12b).

633 $A(x)$ of the IniM differs significantly from that of the RefM both for Estero El
 634 Guindo ($C_{NS\ ref-ini} = 0.080$ and $MAE_{ref-ini} = 0.023$, Fig.14c) and Mercier ($C_{NS\ ref-ini} = 0.313$
 635 and $MAE_{ref-ini} = 0.028$, Fig.14d). This poor representation of the reference $A(x)$ occurs
 636 because there are large areas not segmented in the IniM that contribute directly to specific
 637 locations in the drainage network, which in turns causes major fluctuations of the IniM $A(x)$
 638 functions for both catchments (Fig. 14c, 14d). On the other hand, $A(x)$ of RecM and RefM
 639 are more similar ($C_{NS\ ref-rec} = 0.120$ and $MAE_{ref-rec} = 0.017$ for El Guindo, Fig.14c and C_{NS}
 640 $_{ref-rec} = 0.446$ and $MAE_{ref-rec} = 0.023$ for Mercier, Fig.14d). Although these C_{NS} values are
 641 not very high, the overall shape of $A(x)$ resembles better than of the RefM, particularly as
 642 the large fluctuations previously identified for the IniM are not observed here. Note that
 643 improvements associated with the RecM in Estero El Guindo take place across different
 644 values of x , as bad-shaped elements were homogeneously located throughout the
 645 catchment. In the case of Mercier, bad-shaped elements were mostly located in the upper
 646 zone, so most of the improvements in $W(x)$ and $A(x)$ are observed for the largest values of x .



647

648 **Figure 14. $W(x)$ of El Guindo (a) and Mercier (b) catchments. $A(x)$ of El Guindo (c)**
649 **and Mercier (d) catchments. Each panel shows the results for the IniM (grey dotted**
650 **line), RecM (continuous red line), and RefM (continuous black line).**

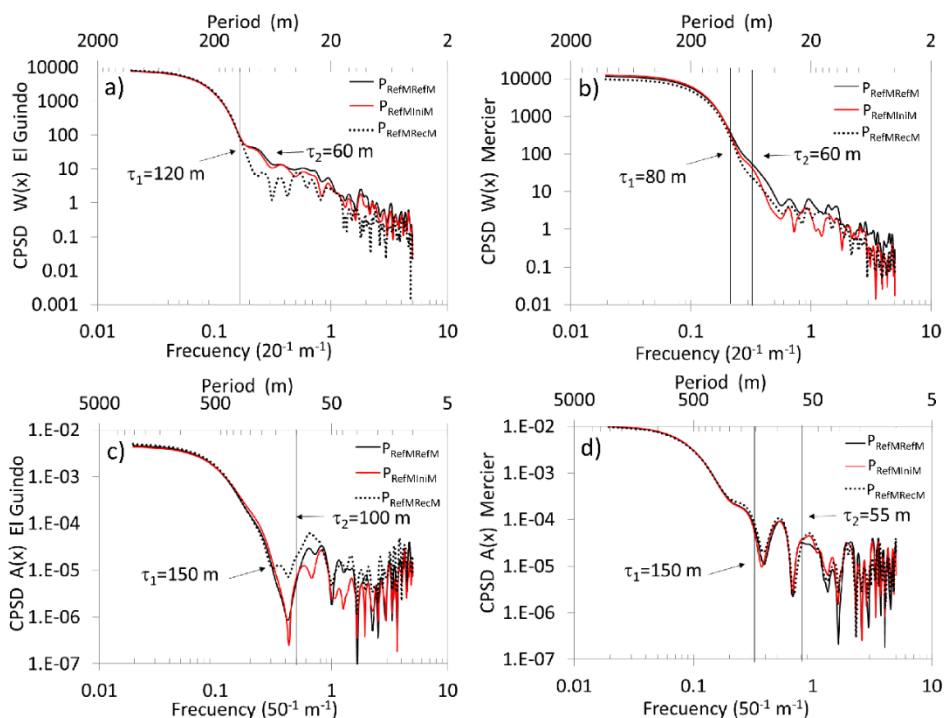
651

652 Fig. 15 shows the CPSD of $W(x)$ and $A(x)$ for both catchments. Here we define
653 $P_{\text{RefM,RefM}}$ as the CPSD between RefM and itself, $P_{\text{RefM,IniM}}$ as the CPSD between RefM and
654 IniM, and $P_{\text{RefM,RecM}}$ as the CPSD between RefM and RecM. The more similar to $P_{\text{RefM,RefM}}$
655 a cross-spectrum is, the more similar the corresponding $W(x)$ or $A(x)$ is to that of the
656 Reference mesh. For $W(x)$ in the Estero El Guindo (Fig.15a), $P_{\text{RefM,RefM}}$ and $P_{\text{RefM,IniM}}$ differ
657 at high frequencies with length scales of $\tau_1 \approx 120$ m or less, whereas $P_{\text{RefM,RefM}}$ and
658 $P_{\text{RefM,RecM}}$ differ for length scales of $\tau_2 \approx 60$ m or less. On the other hand, for the Mercier
659 catchment (Fig.15b) $P_{\text{RefM,RefM}}$ and $P_{\text{RefM,IniM}}$ differ at high frequencies with length scales of
660 $\tau_1 \approx 80$ m or less, whereas $P_{\text{RefM,RefM}}$ and $P_{\text{RefM,RecM}}$ differ for length scales of $\tau_2 \approx 60$ m or
661 less. Hence, in both catchments, the results from the CPSD analysis confirm that $W(x)$ of
662 the RecM is better than that of the IniM in resembling $W(x)$ of the RefM at smaller scales.
663 This improvement is relevant as small-scale features are fundamental in explaining the
664 different mechanisms influencing the hydrologic response of urban catchments (Rossel et
665 al., 2014). Moreover, previous studies concluded that high-frequency components of $W(x)$
666 may be useful for classification of river network topology and regionalization of floods
667 (Richards-Pecou, 2002; Lashermes and Foufoula-Georgiou, 2007, Moussa, 2008).

668 For $A(x)$ in the Estero El Guindo (Fig.15c), $P_{\text{RefM,RefM}}$ and $P_{\text{RefM,IniM}}$ also differ at
669 high frequencies with length scales of $\tau_1 \approx 150$ m or less, whereas $P_{\text{RefM,RefM}}$ and $P_{\text{RefM,RecM}}$
670 differ for length-scales of $\tau_2 \approx 100$ m or less. For the Mercier catchment (Fig.15d) $P_{\text{RefM,RefM}}$
671 and $P_{\text{RefM,IniM}}$ differ at high frequencies with length scales of $\tau_1 \approx 150$ m or less, whereas
672 $P_{\text{RefM,RefM}}$ and $P_{\text{RefM,RecM}}$ differ for length-scales of $\tau_2 \approx 55$ m or less. Again, the results from
673 the CPSD analysis show that $A(x)$ of the RecM resembles better than of RefM at smaller
674 scales than $A(x)$ of IniM.

675 Our results reinforce the idea that the main impacts associated with different terrain
676 representations are observed at small length-scales, typical of residential lots and streets
677 (Sanzana et al., 2013), and that the recommended mesh to represent the terrain is able to
678 minimize these impacts while being efficient in terms of computing time cost. Indeed, using

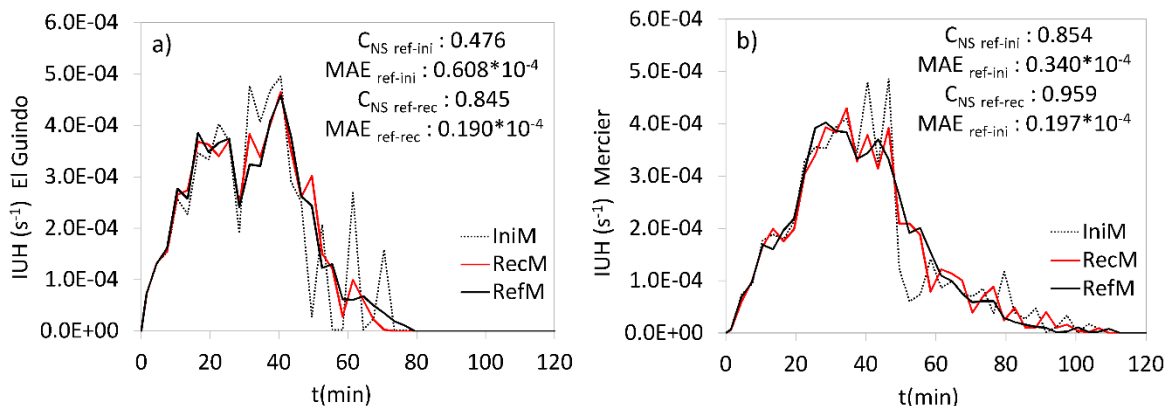
679 geometrical restrictions to generate the terrain meshes for both catchments improved the
 680 representation of the drainage network.
 681



682
 683 **Figure 15. CPSD of $W(x)$ for El Guindo (a) and Mercier (b) catchments. CPSD of $A(x)$**
 684 **for El Guindo (c) and Mercier (d) catchments. Each panel shows the IniM (grey dotted**
 685 **line), RecM (continuous red line), and RefM (continuous black line)**

686
 687 4.2.2. IUH extracted from hydrological meshes

688 The IUHs computed from $A(x)$ of the different drainage networks are presented for
 689 El Guindo (Fig. 16a) and the Mercier (Fig. 16b) catchments. As expected, all the
 690 hydrographs are positively skewed, and the degree of similarity among them is much higher
 691 than for the case of $A(x)$, regardless the drainage network from which they come.
 692 Nonetheless, for both catchments the IUH for RecM resembles much more that of the
 693 RefM than the IniM ($C_{NS\ ref-ini} = 0.476$ vs. $C_{NS\ ref-rec} = 0.845$ for El Guindo, and $C_{NS\ ref-ini} =$
 694 0.854 vs. $C_{NS\ ref-rec} = 0.959$ for Mercier), as part of the fluctuations of $A(x)$ for IniM is
 695 transferred to the corresponding IUHs.



696

697 **Figure 16. IUH derived from IniM, RecM and RefM for El Guindo (a) and Mercier**
 698 **(b) catchments.**

699

700 4.2.3. Discretization error metric

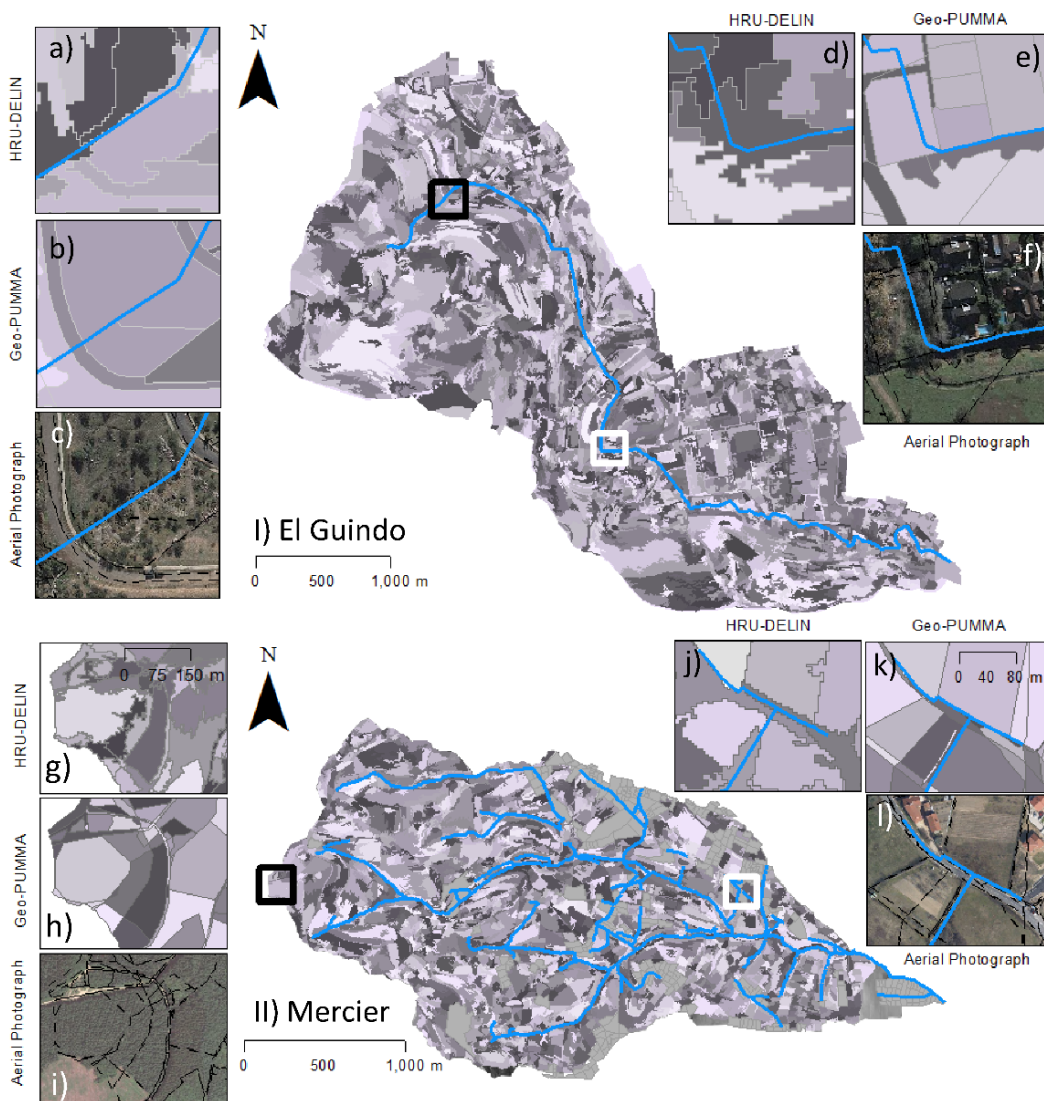
701 After defining RefM as the reference schematic representation in Eq. (1), for each
 702 catchment we computed ΔL_{ini} and ΔL_{rec} of the IniM and RecM respectively. For the Estero
 703 El Guindo, $\Delta L_{ini} = 140-57 = 83$ m and $\Delta L_{rec} = 82-57 = 26$ m, whereas for the Mercier
 704 catchment $\Delta L_{ini} = 91-67 = 24$ m and $\Delta L_{rec} = 77-67 = 10$ m. Hence, for both catchments the
 705 recommended mesh produces a lower discretization error metric, which is in agreement
 706 with the better resemblance with the reference IUH achieved using the recommended mesh.

707

708 4.3. Qualitative comparison of Geo-PUMMA with a classical raster approach

709 Finally, we assessed the results from Geo-PUMMA by comparing the terrain
 710 generated for both catchments with that produced by HRU-DELIN (Tilmant et al., 2015), a
 711 tool that uses the raster approach implemented in GRASS-HRU (Schwartz, 2008). The
 712 implementation of HRU-DELIN used a high resolution 2 m DEM, and considered a
 713 minimum area threshold of 10 m^2 for generating the HRU. For the upstream portion of El
 714 Guindo, Figs. 17a-c illustrate the HRU produced with HRU-DELIN, Geo-PUMMA and the
 715 corresponding aerial photograph, respectively, while Figs. 17 d-f illustrate the same for the
 716 downstream portion of the catchment. Figs. 17 g-i and Figs. 17 j-l present the same for the
 717 upstream and downstream portions of the Mercier catchment, respectively. Because it is a
 718 vectorial polygonal mesh generator, in both catchment some thin features (Figs. 17 a,g) or
 719 physical boundaries (Figs. 17 d,j) not well captured by HRU-DELIN, are preserved by

720 Geo-PUMMA (Fig. 17 b,e and Fig. 17 h,k). Furthermore, despite the huge number of HRUs
721 generated by HRU-DELIN for both catchments (over 30,000 units), some land use features
722 are lost. Geo-PUMMA can represent the terrain with a much more reasonable number of
723 HRU (~ 2,000 HRUs) without major losses of land use features. Overall, these results show
724 that Geo-PUMMA is an appropriate tool to represent urban and peri-urban terrains, while
725 tools such as HRU-DELIN are more suitable for representing medium and regional scales
726 in rural or natural catchments.



727
728 **Figure 17. HRU generated using HRU-DELIN (raster approach) and Geo-PUMMA**
729 **(vectorial approach) in El Guindo (I) and Mercier (II) catchments. Comparisons of**
730 **HRU produced with both tools and the corresponding aerial photograph are**

731 **presented for upstream (a, b, c, g, h, i) and downstream (d, e, f, j, k, l) portions of both**
732 **catchments.**

733

734 5. CONCLUSIONS AND FUTURE WORK

735 This paper presents and describes Geo-PUMMA, a polygonal mesh generation tool
736 for representing urban and peri-urban terrains and create the main inputs for distributed
737 hydrological modeling. Geo-PUMMA considers the main physiographic units available in
738 natural and urban landscapes, represented by means of Hydrological Response Units
739 (HRUs) and Urban Hydrological Elements. The tool allows the generation of high quality
740 polygonal meshes in which the numerous bad-shaped units, created by the initial
741 intersection of GIS maps (land use, soil type, geology, river network), are improved. In
742 particular, the tool succeeds in segmenting non-convex, thin and large elements and
743 assigning more homogeneous properties to the different HRUs in the mesh. Geo-PUMMA
744 represents urban and natural elements and extracts the hydrological interfaces and the
745 drainage network with routing scripts. The generated vectorial mesh and corresponding
746 databases provide useful information for any distributed hydrological model that requires a
747 detailed representation of urban and peri-urban terrains. Geo-PUMMA is a computer-aided,
748 semi-automatic tool, so the active involvement of the modeler is required to obtain good
749 results.

750 Geo-PUMMA was applied to two peri-urban catchments located in different
751 geographical regions (El Guindo, Chile and Mercier, France). We generated three spatial
752 meshes with different degrees of segmentation, defined by threshold values of geometric
753 constraints (i.e convexity index CI , form factor FF and maximum HRU area A_{max}). The
754 quality of the topography and drainage network representation increased with the degree of
755 segmentation, but the computing-time grew as well. For both catchments a recommended
756 mesh was identified, which represented the terrain well without highly increasing the
757 number of HRUs. In addition, this mesh was demonstrated to provide a hydrologic
758 connectivity very similar to that obtained for the most detailed possible representation. This
759 mesh considered threshold values of $CI=0.75$, $FF=0.2$ and $A_{max}=2$ ha, which are
760 recommended for future applications of Geo-PUMMA. Overall, the application to both
761 catchments shows the flexibility of the tool with different geographical conditions.

762 Other examples of decomposition of non-convex polygons into “approximately
763 convex” elements implemented by Lien and Amato (2006) (ACD algorithm) and Liu et al.
764 (2014) (DuDe algorithm) only consider convexity criterion strictly. It would be interesting
765 to compare these geometrical algorithms against the one proposed in Geo-PUMMA, in
766 order to evaluate its possibility to use other geometrical criteria. Moreover, a more detailed
767 analysis could be performed to better assess and justify the threshold values of *CI* and *FF*
768 here proposed, and to improve the computational complexity of the geometrical algorithms
769 developed in Geo-PUMMA.

770

771 ACKNOWLEDGEMENTS

772 This work was developed within the framework of Project MAPA (IDRC 107081-
773 001) and Project ECOS-CONICYT C14U02. Funding from Projects FONDECYT
774 N°1131131, CEDEUS (FONDAP 15110020), FONDECYT ENL009/15 and IRSTEA-Lyon
775 are also acknowledged. Finally Jorge Gironás acknowledge CIGIDEN (FONDAP
776 15110017). The Mercier catchment is part of OTHU (Observatoire de Terrain en
777 Hydrologie Urbaine). This work was partially developed within the framework of the Panta
778 Rhei Research Initiative of the International Association of Hydrological Sciences.

779 **APPENDIX 1:** List of additional GRASS and Geo-MHYDAS commands

780 The following are the additional GRASS and Geo-MHYDAS scripts of optional or
781 compulsory use.

782

783 GRASS GIS Commands

784 **v.generalize:** Vector based generalization. Used to simplify contour and vertexes necessary
785 to represent an irregular shape unit (Optional Tool).

786 **v.clean:** Toolset for cleaning topology of vector map. Used to clean small areas (Optional
787 Tool).

788

789 Geo-MHYDAS Commands

790 **m.snaplp:** Adjusting geometry of linear features. Used to adjust river polyline to the closet
791 boundaries (Optional Tool).

792 **m.seg:** Overlaying geographical objects. Used to create the first intersection of polygons
793 and polylines features (Compulsory Tool).

794 **m.dispolygseg:** Selective dissolving small areal features. Used to dissolve areas with area
795 lower than certain threshold (Optional Tool).

796 **m.sliverpolygseg:** Selective dissolving sliver areal features. Used to dissolve thin and long
797 units (Optional Tool).

```
798  APPENDIX 2: Form Factor segmentation script (p.form_factor.py)
799  1.- For each polygon  $P$  with  $FF \leq FF_{min}$ 
800  2.-    Split boundaries inserting vertex  $d_{max} = 5$  m
801  3.-    Apply Triangle
802  4.-    While P has triangles not yet dissolved
803  5.-        Select triangle with the largest area
804  6.-        Select triangle neighbor with the largest area and create new group  $P'$ 
805  7.-            While  $FF$  of  $P' \geq FF_{min}$ 
806  8.-                Search the neighbor triangles with the largest area
807  9.-                Dissolve boundaries of this group
808  10.-                Compute the  $FF$  of this new group
809  11.-            end while
810  12.-        Update  $P = P - P'$ 
811  13.-    end While
812  14.-    Dissolve areas  $<$  area threshold
813  15.- end For
```

814 **APPENDIX 3: OLAF Algorithm (p.olaf.py)**

- 815 1.- For each sub-catchment S
- 816 2.- Find isolated URH or UHE in the border (only with one neighbor)
- 817 3.- Connect them with nearest neighbor
- 818 4.- Find the URH or UHE which share a boundary with channelized system
- 819 5.- Connect the URH or UHE with channelized drainage
- 820 6.- Find the highest URH or UHE
- 821 7.- Connect it with the lowest neighbor until reaching the channelized system
- 822 8.- If it does not reach the channelized drainage
- 823 9.- Go back one neighbor element upstream
- 824 10.- Connect it with the second lowest neighbor
- 825 11.- If there is a loop
- 826 12.- Go back to the unit upstream the loop
- 827 13.- Connect it with the second lowest neighbor
- 828 14.- Collect all the OLAF path-ways
- 829

830 **REFERENCES**

- 831 Banzhaf, E., Reyes-Paecke, S., Müller, A., Kindler, A., 2013. Do demographic and land-use
832 changes contrast urban and suburban dynamics? A sophisticated reflection on
833 Santiago de Chile. *Habitat International*. 39, 179-191. DOI:
834 10.1016/j.habitatint.2012.11.005
- 835 Bennett, N.D., Croke, G.F.W., Guariso, G., Guillaume, J.H.A., Hamilton, S.H., Jakeman,
836 A.J., Marsili-Libelli, S., Newham, L.T.H., Norton, J.P., Perrin, C., Pierce, S.A.,
837 Robson, B., Seppelt, R., Voinov, A.A., Fath, B.D., Andreassian, V., 2013.
838 Characterizing performance of environmental models. *Environmental Modelling &*
839 *Software*. 40, 1-20. DOI: 10.1016/j.envsoft.2012.09.011
- 840 Bhatt, G., Kumar, M., Duffy, C.J., 2014. A tightly coupled GIS and distributed hydrologic
841 modeling framework. *Environmental Modelling & Software*. 62, 70-84. DOI:
842 10.1016/j.envsoft.2014.08.003
- 843 Bocher, E. and Martin, J.Y., 2012. TAnaTo2: A tool to evaluate the impact of natural and
844 anthropogenic artefacts with a TIN-based model, in Bocher, E., Neteler, M. (Eds.),
845 *Geospatial Free and Open Source Software in the 21st Century*. Springer Berlin
846 Heidelberg, pp. 63-85. DOI: 10.1007/978-3-642-10595-1_5
- 847 Booth, D.B. and Fischenich, C.J., 2015. A channel evolution model to guide sustainable
848 urban stream restoration. *Area*. 47(4), 408-421. DOI: 10.1111/area.12180
- 849 Booth, D.B. and Henshaw, P. C., 2001. Rates of Channel Erosion in Small Urban Streams,
850 in Wigmosta, M. S., Burges, S. J. (Eds.), *Land Use and Watersheds: Human*
851 *Influence on Hydrology and Geomorphology in Urban and Forest Areas*, American
852 Geophysical Union, Washington, D. C. 17-38. DOI: 10.1029/WS002p0017
- 853 Braud, I., Breil, P., Thollet, F., Lagouy, M., Branger, F., Jacqueminet, C., Kermadi, S.,
854 Michel, K., 2013. Evidence of the impact of urbanization on the hydrological
855 regime of a medium-sized periurban catchment in France. *Journal of Hydrology*.
856 485, 5-23. DOI: 10.1016/j.jhydrol.2012.04.049.
- 857 Braud, I., Fletcher, T.D., Andrieu, H., 2013. Hydrology of peri-urban catchments: Processes
858 and modelling. *Journal of Hydrology*. 485, 1-4. DOI: 10.1016/J.hydrol.2013.02.045

- 859 BRGM, 2011. Bureau of Geological and Mining Research. URL:
860 <http://infoterre.brgm.fr/viewer/MainTileForward.do;jsessionid=C6247604415C79>
861 ABC4729563FD5969E [In French, accessed 18.03.16]
- 862 Brossard, F., 2011. Automatisation du pretraitement des donnees spatiales pour la
863 modelisation hydrologique distribuee en zone peri-urbaine [Automatization of
864 preprocessing of spatial information for distributed hydrological modeling in peri-
865 urban zones]. Rapport de Step 2AE. EPMI Ecole D`Ingenieurs. Cemagref-Lyon. 77
866 [In French].
- 867 DGA-AC, 2000. Modelo de simulación hidrológico operacional cuencas de los ríos Maipo
868 y Mapocho [Hydrological modeling for management of Maipo and Mapocho
869 Catchments]. Dirección General de Aguas, División de Estudios y Planificación,
870 Ayala, Cabrera y Asociados Ingenieros Consultores Ltda. [In Spanish].
- 871 DGA-Arrau, 2008. Plan director para la gestión de los recursos hídricos cuenca del río
872 Maipo: fase II actualización del modelo [Master Plan for water resources
873 management of Maipo river: Second Step updating modeling]. Dirección General
874 de Aguas, Ministerio de Obras Públicas de Chile. Arrau Ingeniería. [In Spanish].
- 875 DOH-CADE, 2001. Plan maestro de evacuación y drenaje de aguas lluvias del Gran
876 Santiago [Urban Drainage and Stormwater Master Plan for the Metropolitan area
877 of Santiago]. Dirección de Obras Hidráulicas, Ministerio de Obras Públicas de
878 Chile. CADE Consultores en Ingeniería.[In Spanish].
- 879 Di Luzio, M., Srinivasan, R., Arnold, J.G., 2004. A GIS-coupled hydrological model
880 system for the watershed assessment of agricultural nonpoint and point sources of
881 pollution. Transactions in GIS. 8(1), 113-136. DOI: 10.1111/j.1467-
882 9671.2004.00170.x
- 883 DOH-EIC, 2004. Diagnóstico y proposición plan maestro de manejo de cauces naturales,
884 cuenca del río Mapocho hasta Estero las Hualtatas [Diagnostic and Master Plan
885 proposal for the Management of Mapocho River and Estero Las Hualtatas]. Región
886 Metropolitana. Dirección de Obras Hidráulicas, EIC consultores. [In Spanish].
- 887 Douglas, D.H. and Peucker, T.K., 1973. Algorithms for the reduction of the number of
888 points required to represent a digitized line or its caricature. Cartographica: The

- 889 International Journal for Geographic Information and Geovisualization. 10(2), 112-
890 122. DOI: 10.3138/FM57-6770-U75U-7727
- 891 Flügel, W.A., 1995. Delineating hydrological response units by geographical information
892 system analyses for regional hydrological modelling using PRMS/MMS in the
893 drainage basin of the River Bröl, Germany. Hydrological Processes. 9(3-4), 423-
894 436. DOI: 10.1002/hyp.3360090313
- 895 Fuamba, M., Branger, F., Braud, I., Sanzana Cuevas P., Sarrazin, B., Jankowsky, S., 2015.
896 Interest of spatially distributed data to evaluate the object-oriented PUMMA model
897 on the semi-rural Mercier catchment (Yzeron basin, France), 36th IAHR World
898 Congress, June 28-July 3 2015, Delft, The Hague, The Netherlands, 8 pp,
899 <http://89.31.100.18/~iahrpapers/80490.pdf>
- 900 Geo-PUMMA Team, 2017. Geo-PUMMA Tutorial v.1.
901 <https://forge.irstea.fr/projects/geopumma> [accessed 10.01.17]
- 902 Gironás J., Roesner L.A., Rossman L.A., Davis J., 2010. A new applications manual for the
903 storm water management model (SWMM). Environmental Modelling & Software.
904 25(6), 813–814. DOI: 10.1016/j.envsoft.2009.11.009.
- 905 Gironás, J., Niemann, J.D., Roesner, L.A., Rodriguez, F., and Andrieu, H., 2010. Evaluation
906 of methods for representing urban terrain in storm-water modeling. Journal of
907 Hydrologic Engineering. 15(1), 1-14. DOI: 10.1061/(ASCE)HE.1943-
908 5584.0000142
- 909 Gironás, J., Niemann, J.D., Roesner, L.A., Rodriguez, F., Andrieu, H., 2009. A morpho-
910 climatic instantaneous unit hydrograph model for urban catchments based on the
911 kinematic wave approximation. Journal of Hydrology. 377, 317-334.
912 DOI:10.1016/j.jhydrol.2009.08.030
- 913 GRASS Development Team, 2015. Geographic Resources Analysis Support System
914 (GRASS) Software, Version 6.4. Open Source Geospatial Foundation.
915 <http://grass.osgeo.org> [accessed 18.03.16]
- 916 Haurert, J.H. and Sester, M., 2008. Area collapse and road centerlines based on straight
917 skeletons. GeoInformatica. 12(2), 169-191. DOI: 10.1007/s10707-007-0028-x

- 918 Holmgren, P., 1994. Multiple flow direction algorithms for runoff modelling in grid based
919 elevation models: an empirical evaluation. *Hydrological processes*. 8(4), 327-334.
920 DOI: 10.1002/hyp.3360080405
- 921 Hu, X., Zhang, Z. and Tao, C.V., 2004. A robust method for semi-automatic extraction of
922 road centerlines using a piecewise parabolic model and least square template
923 matching. *Photogrammetric Engineering & Remote Sensing*. 70(12), 1393-1398.
924 DOI: 10.14358/PERS.70.12.1393
- 925 Jacqueminet, C., Kermadi, S., Michel, K., Béal, D., Gagnage, M., Branger, F., Jankowfsky,
926 S. and Braud, I., 2013. Land cover mapping using aerial and VHR satellite images
927 for distributed hydrological modelling of periurban catchments: application to the
928 Yzeron catchment (Lyon, France). *Journal of Hydrology*. 485, 68-83.
929 DOI:10.1016/j.jhydrol.2013.01.028
- 930 Jankowfsky, S., 2011. Understanding and modelling of hydrological processes in small
931 peri-urban catchments using an object oriented and modular distributed approach.
932 Application to the Chaudanne and Mercier sub-catchments (Yzeron Catchment,
933 France). *École Doctorale Terre, Univers, Environnement*. l'Institut National
934 Polytechnique de Grenoble. URL: <http://tel.archives-ouvertes.fr/tel-00721988>.
935 [accessed 18.03.16]
- 936 Jankowfsky, S., Branger, F., Braud, I., Gironás, J. and Rodriguez, F., 2013. Comparison of
937 catchment and network delineation approaches in complex suburban environments:
938 application to the Chaudanne catchment, France. *Hydrological Processes*. 27(25),
939 3747-3761. DOI: 10.1002/hyp.9506
- 940 Jankowfsky, S., Branger, F., Braud, I., Rodriguez, F., Debionne, S., Viallet, P., 2014.
941 Assessing anthropogenic influence on the hydrology of small peri-urban
942 catchments: Development of the object-oriented PUMMA model by integrating
943 urban and rural hydrological models. *Journal of Hydrology*. 517, 1056-1071. DOI:
944 10.1016/j.jhydrol.2014.06.034
- 945 Kass, M., Witkin, A., Terzopoulos, D., 1988. Snakes: Active contour models. *International*
946 *journal of computer vision*. 1(4), 321-331. DOI: 10.1007/BF00133570
- 947 Lagacherie, P., Rabotin, M., Colin, F., Moussa, R., Voltz, M., 2010. Geo-MHYDAS: a
948 landscape discretization tool for distributed hydrological modeling of cultivated

- 949 areas. Computers & Geosciences. 36(8), 1021-1032. DOI:
950 10.1016/j.cageo.2009.12.005
- 951 Lashermes, B. and Foufoula-Georgiou, E., 2007. Area and width functions of river
952 networks: New results on multifractal properties. Water resources research. 43(9),
953 1-19. DOI: 10.1029/2006WR005329.
- 954 Lashermes, B., Foufoula-Georgiou, E., Dietrich, W. E., 2007. Channel network extraction
955 from high resolution topography using wavelets. Geophysical Research Letters. 34,
956 L23S04. DOI:10.1029/2007GL031140.
- 957 Legates, D.R., McCabe, G.J., 1999. Evaluating the use of "goodness-of-fit" measures in
958 hydrologic and hydroclimatic model validation. Water Resources Research. 35(1),
959 233-241. DOI: 10.1029/1998WR900018.
- 960 Lee, J.G. and Heaney, J.P., 2003. Estimation of urban imperviousness and its impacts on
961 storm water systems. Journal of Water Resources Planning and Management.
962 129(5), 419-426. DOI: 10.1061/(ASCE)0733-9496(2003)129:5(419)
- 963 Leninisha, S. and Vani, K., 2015. Water flow based geometric active deformable model for
964 road network. ISPRS Journal of Photogrammetry and Remote Sensing. 102, 140-
965 147. DOI:10.1016/j.isprsjprs.2015.01.013
- 966 Lien, J.-M. and Amato, N.M., 2006 Approximate convex decomposition of polygons.
967 Computational Geometry Theory and Applications. 35(1), pp. 100–123.
968 DOI:10.1016/j.comgeo.2005.10.005
- 969 Liu, G., Xi, Z., and Lien, J. M., 2014. Dual-space decomposition of 2d complex shapes. In
970 Proceedings of the IEEE Conference on Computer Vision and Pattern Recognition.
971 pp. 4154-4161.
- 972 Liu, H., Tolson, B.A., Craig, J.R., Shafii, M. 2016. A priori discretization error metrics for
973 distributed hydrologic modeling applications. Journal of Hydrology. 543, Part B,
974 873–891. DOI: 10.1016/j.jhydrol.2016.11.008
- 975 Moussa, R., 2008. What controls the width function shape, and can it be used for channel
976 network comparison and regionalization? Water Resources Research. 44: W08456.
977 DOI:10.1029/2007WR006118.
- 978 Moussa, R., Voltz, M., Andrieux, P., Lagacherie, P., 2000. Hydrological modelling of a
979 farmed Mediterranean catchment. In: Claps, P., Siccardi, F. (Eds.), Proceedings of

- 980 Mediterranean Storms, European Geophysical Society Plinius Conference'99,
981 Maratea, Italy, pp.377–386.
- 982 Municipalidad de Lo Barnechea, 2012. Plan Regulador Comunal [Municipal Master Plan]
983 URL: http://www.lobarnechea.cl/newweb/mi_comuna/plan_regulador.php [In
984 Spanish, Accessed 22.02.16]
- 985 Nash, J.E. and Sutcliffe, J.V., 1970. River flow forecasting through conceptual models part
986 I—A discussion of principles. *Journal of hydrology*. 10(3), 282-290. DOI:
987 10.1016/0022-1694(70)90255-6
- 988 O'Callaghan, J.F. and Mark, D.M., 1984. The extraction of drainage networks from digital
989 elevation data. *Computer vision, graphics, and image processing*. 28(3), 323-344.
990 DOI: 10.1016/S0734-189X(84)80011-0
- 991 Ogden, F.L., Raj Pradhan, N., Downer, C.W., Zahner, J.A., 2011. Relative importance of
992 impervious area, drainage density, width function, and subsurface storm drainage
993 on flood runoff from an urbanized catchment. *Water Resources Research*, 47,
994 W12503, DOI: 10.1029/2011WR010550.
- 995 Neitsch, S.L., Arnold J.G., Kiniry J.R., Williams JR., 2005. Soil and Water Assessment
996 Tool, Theoretical Documentation, Texas Water Resources Institute: College
997 Station, TX.
- 998 Paillé, Y., 2010. Conceptualisation et modélisation d'une base de données en vue de son
999 implémentation dans un modèle hydrologique distribué [Conceptualization and
1000 modeling of spatial information for distributed hydrological modeling]. *Mémoire*
1001 *de Master 2 Cartographie et Gestion des Espaces à Fortes Contraintes*, Université
1002 de Nantes, 50 pp. [In French].
- 1003 Passalacqua, P., Do Trung, T., Fofoula-Georgiou, E., Sapiro, G., Dietrich, W.E., 2010. A
1004 geometric framework for channel network extraction from lidar: Nonlinear
1005 diffusion and geodesic paths. *Journal of Geophysical Research*. 115, F01002.
1006 DOI:10.1029/2009JF001254.
- 1007 Pavez, E.F., Lobos, G.A., Jaksic, F.M., 2010. Long-term changes in landscape and in small
1008 mammal and raptor assemblages in central Chile. *Revista Chilena de Historia*
1009 *Natural*. 83(1), 99-111. DOI: 10.4067/S0716-078X2010000100006.

- 1010 Puente, C.E. and Sivakumar, B., 2003. A deterministic width function model. *Nonlinear*
1011 *Processes in Geophysics*. 10 (6), 525-529.
- 1012 QGIS Development Team, 2015. QGIS Geographic Information System. Open Source
1013 Geospatial Foundation Project. Technical report. URL: <http://qgis.osgeo.org>.
- 1014 Richards-Pecou, B., 2002. Scale invariance analysis of channel network width function and
1015 possible implications for flood behaviour. *Hydrological Sciences Journal*. 47(3),
1016 387-404. DOI: 10.1080/02626660209492942
- 1017 Rodriguez, F., Andrieu, H., Morena, F., 2008. A distributed hydrological model for
1018 urbanized areas – model development and application to case studies. *Journal of*
1019 *Hydrology*. 351, 268–287. DOI: 10.1016/j.jhydrol.2007.12.007.
- 1020 Rodriguez, F., Bocher, E. and Chancibault, K., 2013. Terrain representation impact on
1021 periurban catchment morphological properties. *Journal of Hydrology*. 485, 54-67.
1022 DOI: 10.1016/j.jhydrol.2012.11.023
- 1023 Rodriguez-Iturbe, I., Rinaldo, A., 1997. *Fractal River Basins: Chance and Self organization*,
1024 Ed. Cambridge University Press, New York. 564 pp.
- 1025 Romero ,H., and Vásquez, A., 2005. Evaluación ambiental del proceso de urbanización de
1026 las cuencas del piedemonte andino de Santiago de Chile [Environmental
1027 Evaluation of the urban growth in the Andean piedmont catchments of Santiago de
1028 Chile]. *EURE*, 31(94), 97-117. DOI:10.4067/S0250-71612005009400006.
- 1029 Romero H., Ihl M., Rivera A., Zalazar P., Azocar P., 1999. Rapid urban growth, land-use
1030 changes and air pollution in Santiago, Chile. *Atmospheric Environment*. 33 (24–
1031 25), 4039–4047. DOI: 10.1016/S1352-2310(99)00145-4
- 1032 Romero, H., Salgado, M., Smith, P., 2010. Cambios climáticos y climas urbanos:
1033 Relaciones entre zonas termales y condiciones socioeconómicas de la población de
1034 Santiago de Chile [Climate Change and Urban Climate: Relations between thermal
1035 zones and the socioeconomic conditions of the population of Santiago de Chile].
1036 *Revista INVI*. 25(70), 151-179. [In Spanish] DOI:10.4067/S0718-
1037 83582010000300005
- 1038 Rossel, F., Gironás, J., Mejía, A., Rinaldo, A., Rodriguez, F., 2014. Spatial characterization
1039 of catchment dispersion mechanisms in an urban context. *Advances in Water*
1040 *Resources*. 74, 290-301. DOI: 10.1016/j.advwatres.2014.09.005

- 1041 Sangireddy, H., C.P. Stark, A. Kladzyk, P. Passalacqua, 2016. GeoNet: An open source
1042 software for the automatic and objective extraction of channel heads, channel
1043 network, and channel morphology from high resolution topography data.
1044 Environmental Modeling and Software. 83, 58-73, DOI:
1045 10.1016/j.envsoft.2016.04.026.
- 1046 Santo Domingo, N., Refsgaard, A., Mark, O., Paludan, B., 2010. Flood analysis in mixed-
1047 urban areas reflecting interactions with the complete water cycle through coupled
1048 hydrologic–hydraulic modelling. Water Science and Technology. 62(6), 1386-1392.
1049 DOI: 10.2166/wst.2010.365
- 1050 Sanzana, P., Jankowfsky, S., Branger, F., Braud, I., Vargas, X., Hitschfeld, N., Gironás, J.,
1051 2013. Computer-assisted mesh generation based on hydrological response units for
1052 distributed hydrological modeling. Computers & Geosciences. 57, 32-43. DOI:
1053 10.1016/j.cageo.2013.02.006
- 1054 Sarrazin, B., 2012. Approches spatiales pour décrire le réseau de drainage et suivre sa
1055 dynamique de fonctionnement en milieu rural dans une perspective d'aide à la
1056 modélisation hydrologique (Spatial approaches to describe the drainage system and
1057 follow its dynamics operating in rural areas with a view to support hydrologic
1058 modeling). Ph.D. Dissertation, École Doctorale Terre, Univers, Environnement.
1059 l'Institut National Polytechnique de Grenoble, [In French].
- 1060 Schwartze, C., 2008. Deriving Hydrological Response Units (HRUs) using a Web
1061 Processing Service implementation based on GRASS-GIS. Geoinformatics FCE
1062 CTU 2008. Workshop Proceedings. 3, 67-78.
- 1063 Seibert, J. and McGlynn, B.L., 2007. A new triangular multiple flow direction algorithm for
1064 computing upslope areas from gridded digital elevation models. Water Resources
1065 Research. 43(4), WO4501. DOI: 10.1029/2006WR005128
- 1066 Shewchuck, J., 1996. Triangle: Engineering a 2D Quality Mesh Generator and Delaunay
1067 Triangulator, in Lin, M.C., Manocha, D., (Eds.), Applied Computational Geometry:
1068 Towards Geometric Engineering. Berlin, Heidelberg. 1148, 203-222. DOI:
1069 10.1007/BFb0014497

- 1070 Shuster, W.D., Bonta, J., Thurston, H., Warnemuende, E., Smith, D.R., 2005. Impacts of
1071 impervious surface on watershed hydrology: a review. *Urban Water Journal*. 2(4),
1072 263-275. DOI: 10.1080/15730620500386529
- 1073 Shynk, J. J., 2012. *Probability, Random Variables, and Random Processes: Theory and*
1074 *Signal Processing Applications.*, first ed. Wiley-Interscience. New-Jersey.
- 1075 Singh, V. P., 1995. Chapter 1: Watershed Modeling, in Singh, V.P., (Ed.), *Computer Models*
1076 *of Watershed Hydrology*, Water Resource Publications. 1-22.
- 1077 SIRA, 2011. Soil Information of Rhône-Alpes. URL: [http://www.rhone-](http://www.rhone-alpes.chambagri.fr/sira/)
1078 [alpes.chambagri.fr/sira/](http://www.rhone-alpes.chambagri.fr/sira/). [Accessed 31.03.16]
- 1079 Smith, J.A., Baeck, M.L., Morrison, J.E., Sturdevant-Rees, P., Turner-Gillespie, D.F., Bates,
1080 P.D., 2002. The regional hydrology of extreme floods in an urbanizing drainage
1081 basin. *Journal of Hydrometeorology*. 3(3), 267-282. DOI:10.1175/1525-
1082 7541(2002)003<0267:TRHOEF>2.0.CO;2
- 1083 Smith, J.A., Baeck, M.L., Meierdiercks, K.L., Nelson, P.A., Miller, A.J., Holland, E.J.,
1084 2005. Field studies of the storm event hydrologic response in an urbanizing
1085 watershed. *Water Resources Research*. 41, W10413. doi:10.1029/2004WR003712.
- 1086 Tilmant, F., Gouttevin, I., Barachet, C., Montginoul, M., Branger, F., Leblois, E., Sauquet,
1087 E., Braud, I., Noël, D., Le Gros, C., 2015. Modélisation hydrologique distribuée du
1088 Rhône [A distributed hydrological model of the Rhône catchment]. Technical
1089 Report. [In French], 105 pp.
- 1090 Toma, L., Wickremesinghe, R., Arge, L., Chase, J.S., Vitter, J.S., Halpin, P.N. and Urban,
1091 D., 2001. Flow computation on massive grids. In *Proceedings of the 9th ACM*
1092 *international symposium on Advances in geographic information systems*, 82-87.
1093 DOI: 10.1145/512161.512180
- 1094 Urban Drainage and Flood Control District (UDFCD), 2001. *Urban Storm Drainage*
1095 *Criteria Manual*. Revised August 2006, Denver, Colorado.
1096 URL:www.udfcd.org/downloads/down_critmanual.ht.
- 1097 Veneziano, D., Moglen, G.E., Furcolo, P., Iacobellis, V., 2000. Stochastic model of the
1098 width function. *Water Resources Research*. 36(4), 1143-1157. DOI:
1099 10.1029/2000WR900002

- 1100 Vietz, G. J., Walsh, C. J., Fletcher, T. D., 2015. Urban hydrogeomorphology and the urban
1101 stream syndrome: Treating the symptoms and causes of geomorphic change.
1102 Progress in Physical Geography. 24(3), 706-723. DOI:
1103 10.1177/0309133315605048.
- 1104 Viviroli, D., Zappa, M., Gurtz, J., Weingartner, R., 2009. An introduction to the
1105 hydrological modelling system PREVAH and its pre-and post-processing-tools.
1106 Environmental Modelling & Software. 24(10), 1209-1222. DOI:
1107 10.1016/j.envsoft.2009.04.001.